International Journal of Earth Sciences (2021) 110:377–398
https://doi.org/10.1007/s00531-020-01957-y

ORIGINAL PAPER

Latest Carboniferous to early Permian volcano-stratigraphic evolution in Central Europe: U–Pb CA–ID–TIMS ages of volcanic rocks in the Thuringian Forest Basin (Germany)

Harald Lützner[1] · Marion Tichomirowa[2] · Alexandra Käßner[2] · Reinhard Gaupp[1]

Received: 16 April 2020 / Accepted: 28 October 2020 / Published online: 23 November 2020

Abstract
Mainly acidic Stephanian to early Permian volcanic rocks and intercalated sediments accumulated in the Thuringian Forest Basin (TFB) in central Germany to a total thickness of ca. 2000 m. This basin offers a wide range of biostratigraphic information. New high-precision U–Pb CA–ID–TIMS (chemical abrasion–isotope dilution–thermal ionization mass spectrometry) zircon data are obtained from volcanic rocks for the first time in the TFB. Pre-treatment of the zircons by chemical abrasion was important to get rid of severe Pb loss. The zircon ages of the investigated formations indicate that the total duration of the volcanic activity in the TFB was considerably shorter [ca. 4 Myr: from 300 Ma for the oldest formation (Möhrenbach) until ca. 296 Ma for the youngest volcanic-rock-bearing formation (Rotterode)] than suggested in previous studies (ca. 20 Myr; 295 Ma to 275 Ma). Consequently, the well-documented gap of the sedimentary record from the early Permian volcanic rocks up to the Illawarra geomagnetic reversal has to be extended to ca. 25 Myr from the previously proposed 5 Myr. The zircon ages of the investigated volcanic rocks allow the constraining of some intercalated fossiliferous horizons crucial for biostratigraphic correlation of latest Carboniferous–early Permian (Rotliegend) sections. The high-precision age data require a new interpretation of the evolution of the TFB but also offer the chance to obtain a more reliable comparison of the timing of the main magmatic activity across intramontane basins as well as to obtain links to the Standard Global Stratigraphic Scale.

Keywords Geochronology · Zircon · Stratigraphy · ID–TIMS · Variscides · Thuringian forest

Introduction

From the late Carboniferous to the early Permian, the transition from the final stage of the Variscan orogeny to the stable continental regime of Pangea in Central Europe led to a change from compressive regimes to extensional/transtensional ones (Ziegler 1990; van Wees et al. 2000; McCann et al. 2006; Timmerman 2008; Kroner et al. 2016, 2020). Paleogeographically, large marine areas of high sea level turned into shallow marine marginal seas, merging in fringes of extensive swamp forests which fossilized to coal measures of Namurian to Westphalian age. In the latest Carboniferous (Stephanian), the humid environments became drier and fluviolacustrine sedimentation took place (e.g., Roscher and Schneider 2006; Paul 2012). Similar sedimentary sequences developed in elongated troughs inside the orogenic belt as in the Saar–Nahe Basin (e.g., Boy et al. 2012) or in the Thuringian Forest Basin (TFB) (Lützner et al. 2012). During the early Permian, these intramontane basins continued to form and fill up due to exhumation and erosion of the Variscan orogen, increasingly under the control of fault tectonics and magmatism.

The TFB is situated in a central and important geographic position in the Variscan orogenic belt in the Mid-German Crystalline Rise and Saxothuringian Zone between the Saar–Nahe and Kraichgau Basins in the SW and the Saale Basin in the NE (Lützner and Kowalczyk 2012; Andreas 2014). These basins were thoroughly studied during the last > 70 years for their geological structure, volcano-sedimentary successions (e.g., Lützner et al. 2012), magnetostratigraphy (e.g., Menning and Bachtadse 2012), and biostratigraphy (e.g., Martens 2012; Schneider and

✉ Marion Tichomirowa
tichomir@mineral.tu-freiberg.de

[1] Institute of Earth Sciences, Friedrich-Schiller-University Jena, Burgweg 11, 07749 Jena, Germany

[2] Institute of Mineralogy, TU Bergakademie Freiberg, Brennhausgasse 14, 09599 Freiberg, Germany

Werneburg 2012). Therefore, they are considered type sections with which the late Carboniferous to Permian/Triassic time period can be studied in detail. In particular, the TFB includes the Carboniferous–Permian boundary and the transition from the late Permian to the Triassic. Besides numerous small gaps in sedimentation, there was a long-lasting middle Permian hiatus detected in previous studies that is present in diverse European basins, particularly in the central Southern Permian Basin in Northern Germany (e.g., van Wees et al. 2000; Geißler et al. 2008). In parts of mid-European basins, sedimentation restarted close to the major geomagnetic Illawarra Reversal (e.g., Hounslow and Balabanov 2018) in the Late Permian. Therefore, because it covers important intervals of Permian sedimentation and non-sedimentation ("intra-Rotliegend hiatus"), the TFB is exceptionally well suited to further our understanding of sediment fill and magmatism during late Paleozoic geodynamic evolution.

Geochronological studies have already been performed in the TFB (Goll and Lippolt 2001; Lippolt et al. 2009; Lützner et al. 2007; Zeh and Brätz 2000), in the Saar–Nahe Basin (von Seckendorff 2012), and in the Saale Basin (Breitkreuz et al. 2009). However, recent developments in zircon U–Pb CA–ID–TIMS (chemical abrasion–isotope dilution–thermal ionization mass spectrometry) dating allow precise determination of crystallization ages with an accuracy of 0.1% (Condon et al. 2015; Schaltegger et al. 2015). This method is, thus, particularly well suited to establish chronological sequences of sedimentary basins if zircon-bearing volcanic intercalations are available. We present new geochronological data from seven felsic volcanic rock samples of the TFB with zircons dated by the U–Pb CA–ID–TIMS method to:

1. Define the age range of volcanic activity in the TFB and compare it to the existing biostratigraphic data,
2. Constrain the gap between the end of major volcanic activity with associated intramontane sediments and the voluminous post-Illawarra paleomagnetic Reversal sediment accumulation of the late Permian stage, and,
3. To compare the timing of the main volcanic activity across Permian basins in Central Europe.

Geological setting

Carboniferous–Permian volcanism in Central Europe

At the end of the Variscan orogeny, an extensive phase of Carboniferous–Permian magmatism led to the extrusion of thick volcanic successions across Europe and NW Africa (Fig. 1a, e.g., Oslo Rift, Scotland, England, Southern Permian Basin/N Germany, W and central Germany, Saxony, N Bohemia, NW part of the Polish Basin, SW Poland, NE Czech Republic, N Spain, Morocco, France, N Italy), with a maximum volume in the late Carboniferous (Stephanian) to early Permian. The eruption of volcanic rocks was accompanied by massive synextensional granitic intrusions and hydrothermal mineralisation (Lorenz and Nicholls 1976, 1984; Hoth et al. 1993; Marx 1995; Marx et al. 1995; Benek et al. 1996; Doblas et al. 1998; Breitkreuz and Kennedy 1999; Lorenz and Haneke 2004; Timmerman 2004, 2008; McCann et al. 2006; Breitkreuz et al. 2007, 2009; Geißler et al. 2008; von Seckendorff 2012; Hoffmann et al. 2013; Willcock et al. 2013; Schmiedel et al. 2015).

In Europe, Stephanian to Permian wrenching resulted in thermal destabilization of the lithosphere, intense fracturing of the crust, disruption and erosion of its sedimentary cover, and regional uplift in the area of the future Southern Permian Basin (van Wees et al. 2000; Kroner et al. 2016). Transtension led to the formation of more than 70 rift basins across Europe. In the North German Basin (as part of the Southern Permian Basin), volcanism between ca. 300 and 290 Ma is closely related in time and space to an episode of major tectonic activity (right-lateral WNW- to W-trending transtensional strike-slip movements; Plein 1993; Gast and Gundlach 2006; McCann et al. 2006). The extensional tectonics were important for supplying pathways for intrusive and extrusive magmas.

The origin of the extensive and voluminous Carboniferous–Permian magmatism in Central Europe has been hotly debated for more than 30 years with diverse theories arising (see, e.g., Doblas et al. 1998; Timmerman 2004; McCann et al. 2006; Geißler et al. 2008). This is partly due to the large geochemical and mineralogical variety of the plutonic and volcanic rocks, but likely also due to the structural and lithospheric complexity of this part of Variscan Europe (Lorenz and Nicholls 1976, 1984; Breitkreuz and Kennedy 1999; Breitkreuz and Mock 2004; von Seckendorff 2004, 2012; McCann et al. 2006; Breitkreuz et al. 2007, 2009). A superplume has been invoked by Doblas et al. (1998) as a background mechanism of this magmatic episode. Rifting, thinning of highly asymmetric lithosphere, local decompression, and lithospheric mantle as the major source of the middle European Carboniferous–Permian volcanic rocks were defined by Neumann et al. (2004). Mantle sources metasomatized by subduction-related material were inferred by Timmerman (2004) to explain the geochemical character of the volcanic rocks in NE Germany that does not agree with an intra-plate setting.

The widespread Stephanian–early Permian (305–285 Ma, Kasimovian–late Artinskian) alkaline to calc-alkaline intrusive and extrusive magmatism of the central European Variscan area and its northern foreland (e.g., the North German Volcanic Complex) is, based on trace element ratios, mantle-derived and shows evidence of moderate crustal contamination (e.g., Marx et al. 1995; Benek et al. 1996; Breitkreuz

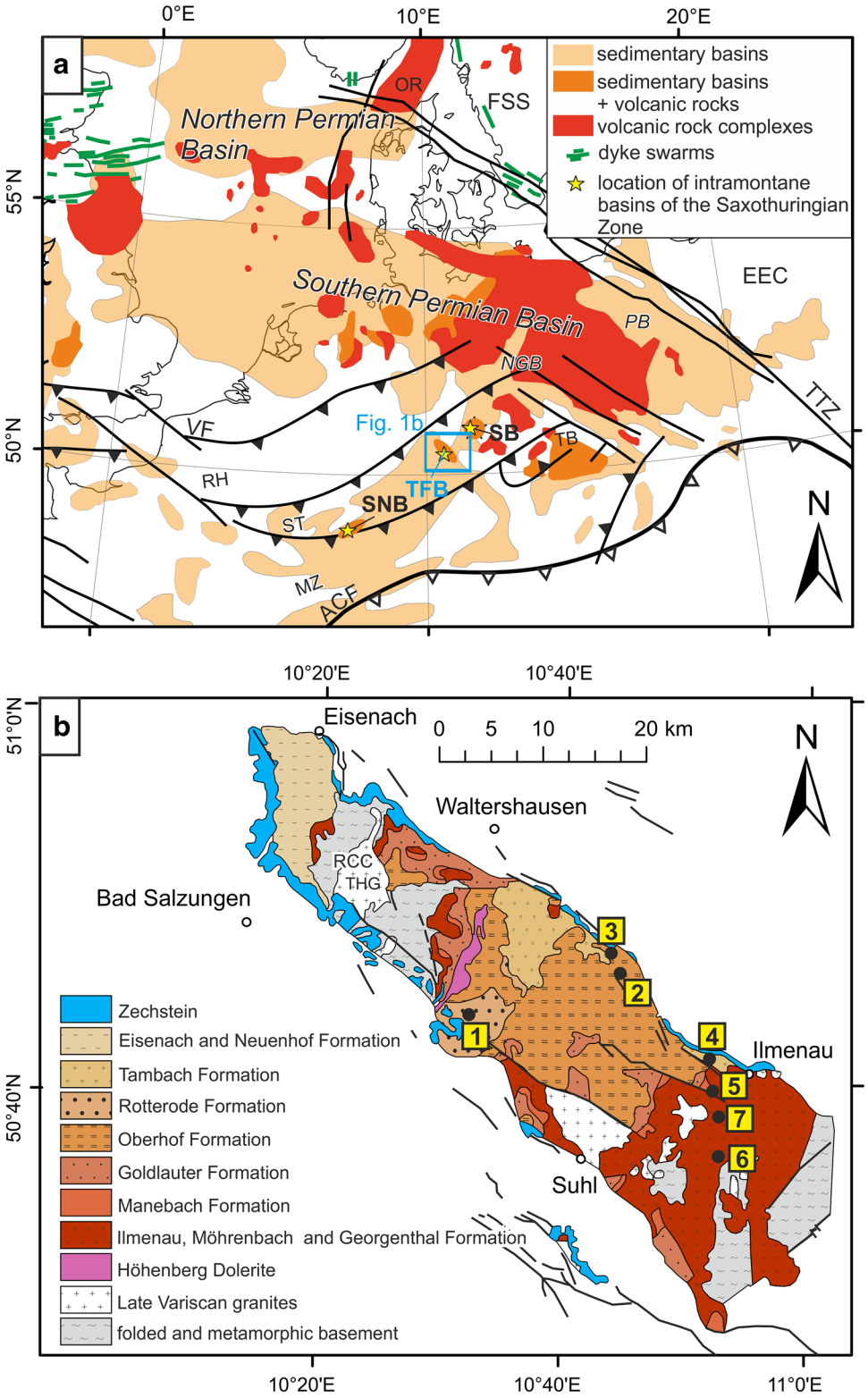

Fig. 1 Simplified geological maps. **a** Geological map of the main tectonic elements of Central Europe in relation to the distribution of Late Carboniferous and Early Permian sedimentary basins and volcanic rocks (based on McCann et al. 2006; Mazur et al. 2010). Major tectonic elements are *ACF* Alpine–Carpathian front, *VF* Variscan deformation front, *RH* Rheno-Hercynian Zone, *ST* Saxothuringian Zone, *MZ* Moldanubian Zone, *TB* Tepla–Barrandian Zone, *EEC* East European Platform, *FSS* Fennoscandian Shield, *TTZ* Tornquist–Teisseyre Zone, *OR* Oslo Rift. Two sub-basins of the Southern Permian Basin are labeled as *NGB* North German Basin, *PB* Polish Basin, and the main sedimentary basins of the Saxothuringian Zone are *SNB* Saar–Nahe Basin, *TFB* Thuringian Forest Basin, *SB* Saale Basin. Thick black lines are tectonic elements; thin black lines represent the coastlines of Central Europe. **b** Geological Map of the Thuringian Forest Basin. Sample locations for new zircon U–Pb CA–ID–TIMS dating are shown by black circles with sample numbers in yellow boxes. (Lützner et al. 2012, amended). *RCC* Ruhla Crystalline Complex, *THG* Thüringer Hauptgranit

and Kennedy 1999; McCann et al. 2006). In the internal Variscides (South of the Variscan front, VF in Fig. 1a), mafic rocks are rare with felsic-intermediate compositions being dominant; whereas in the external areas, calc-alkaline SiO_2-rich volcanic rocks are more common (e.g., Timmerman 2008).

The late Stephanian to earliest Permian sequence (volcano-sedimentary and volcanic rocks as well as clastic fill)

reached its maximum thickness in the TFB (ca. 2000 m, a value comparable to maxima in N Germany.) The igneous rocks are lavas and pyroclastic rocks of mainly trachyandesitic to rhyolitic composition (Andreas et al. 1974; Obst et al. 1999; Obst and Katzung 2000; Lützner et al. 2007, 2012).

Thuringian forest basin (TFB)

Geological overview

The TFB is of exceptional value for the age determination of late Variscan Carboniferous–Permian basins because it is well investigated concerning lithostratigraphy (Lützner et al. 2012) and biostratigraphy (e.g., Schneider and Werneburg 2012; Schneider et al. 2020). The TFB also shows recurrent strong intra-basinal volcanism that produced piles of lava flows and tuffs hundreds of meters thick. Precise and accurate age dating of the TFB formations is, therefore, critical for the correct correlation and stratigraphic categorisation of a variety of other European late Carboniferous/early Permian basins.

Tectonically, the Thuringian Forest represents an uplifted block bordered by mainly NW–SE-striking faults and flexures that predominantly coincide with the morphological slopes of the range. The maximum altitudes are reached in the middle part (Großer Beerberg, 982 m) and in the northwest (Großer Inselsberg, 916 m), with decreasing altitudes (ca. 700 m) between both peaks and further to the southeast. The forelands are made up of Triassic sedimentary formations (Buntsandstein, Muschelkalk, Keuper), in part with a narrow strip of late Permian Zechstein deposits along marginal flexures; whereas, within the elevated range, Stephanian and early Permian successions and their Variscan basement are revealed (Fig. 1b).

The Stephanian–Rotliegend (late Carboniferous–early Permian) filling of the TFB disconformably overlies the Variscan basement. On the southeastern margin, the basement consists of Proterozoic and Paleozoic up to lower Carboniferous sedimentary units of the Saxothuringian Zone which were folded and underwent a low-grade Variscan metamorphism (Bankwitz and Bankwitz 2003; Meinel 2003).

To the northwest, the basin filling covers the "Thüringer Hauptgranit", an early post-kinematic granite pluton of early Carboniferous age (330.3 ± 3.4 Ma to 337 ± 4 Ma from zircon Pb–Pb evaporation and dark mica Ar–Ar, and K–Ar dating; Zeh and Brätz 2000; Zeh et al. 2000; Goll and Lippold 2001) with a contact belt against the early Paleozoic in the Southeast (Fig. 1b; Bankwitz and Kaemmel 1957). The composition of the "Thüringer Hauptgranit" is heterogeneous and varies between quartzdioritic, granodioritic, and leucogranitic (Meinel 2003). These plutonic rocks had been eroded and deeply weathered before the development of the TFB (Lützner et al. 2012). The extension of the TFB spreads beyond the recent tectonic borders of the Thuringian Forest at least 12 km to the Northeast (borehole Gotha 1), and at least 20 km to the Southwest (boreholes Metzels, Thüringen Süd, Rannungen, not shown in Fig. 1). The extension to the NW is bordered by the Ruhla Crystalline Complex (RCC, Fig. 1b). Paleocurrent patterns indicate that the RCC was one of the source areas for the TFB sedimentary formations.

Lithostratigraphy

Figure 2 illustrates the lithostratigraphic subdivisions of the TFB. The lowermost formations (Georgenthal Formation in the NW and Möhrenbach Formation in the SE, thought to be coeval) reflect a first culmination of magmatic activity and are both dominated by intermediate volcanic rocks with additional rhyolites present in the Möhrenbach Formation. Thin sedimentary intercalations were used for internal correlations (Lützner et al. 2012: p. 430; Andreas 2014: p. 96). The overlying Ilmenau Formation displays local sedimentary beds alternating with volcanic and pyroclastic rocks of bimodal basaltic and rhyolitic composition (Lützner et al. 2012).

Extrusive volcanic rocks are extremely scarce in the two subsequent formations, i.e., in the coal-bearing Manebach Formation and in the fluvial–lacustrine Goldlauter Formation. Volcanic events are restricted to several tuff layers, which are used as tephrostratigraphic marker horizons (Andreas and Haubold 1975).

In the TFB, a second culmination of Rotliegend volcanism occurred during the following Oberhof Formation where volcanic rocks alternate with volcaniclastics and subordinately with alluvial red beds and lacustrine gray beds. The basal group of volcanic rocks within the Oberhof Formation consists of an association of basic, intermediate, and acidic volcanic rocks that is intercalated within the lower sedimentary beds of fluvial and lacustrine origin. The middle and upper parts of the Oberhof Formation are dominated by rhyolites and associated volcaniclastics. So-called Older Rhyolites prevail in the middle part. They are characterized by medium to large feldspar phenocrysts. Finally, the so-called Younger Rhyolites constitute the upper part of the Oberhof Formation. These rocks have typically small qtz–fsp phenocrysts of about 1 mm size. However, a few rhyolite domes intruding the Younger Rhyolite level also have large qtz–fsp phenocrysts.

The Rotterode Formation consists of red sandstones with conglomeratic intercalations that surround several rhyolitic bodies and tuff layers. This formation was deposited on the Oberhof Formation with a low-angle unconformity separating the two formations. The angular unconformity was likely related to the tectonically induced uplift of the Ruhla crystalline complex, which caused rejuvenation of the relief and

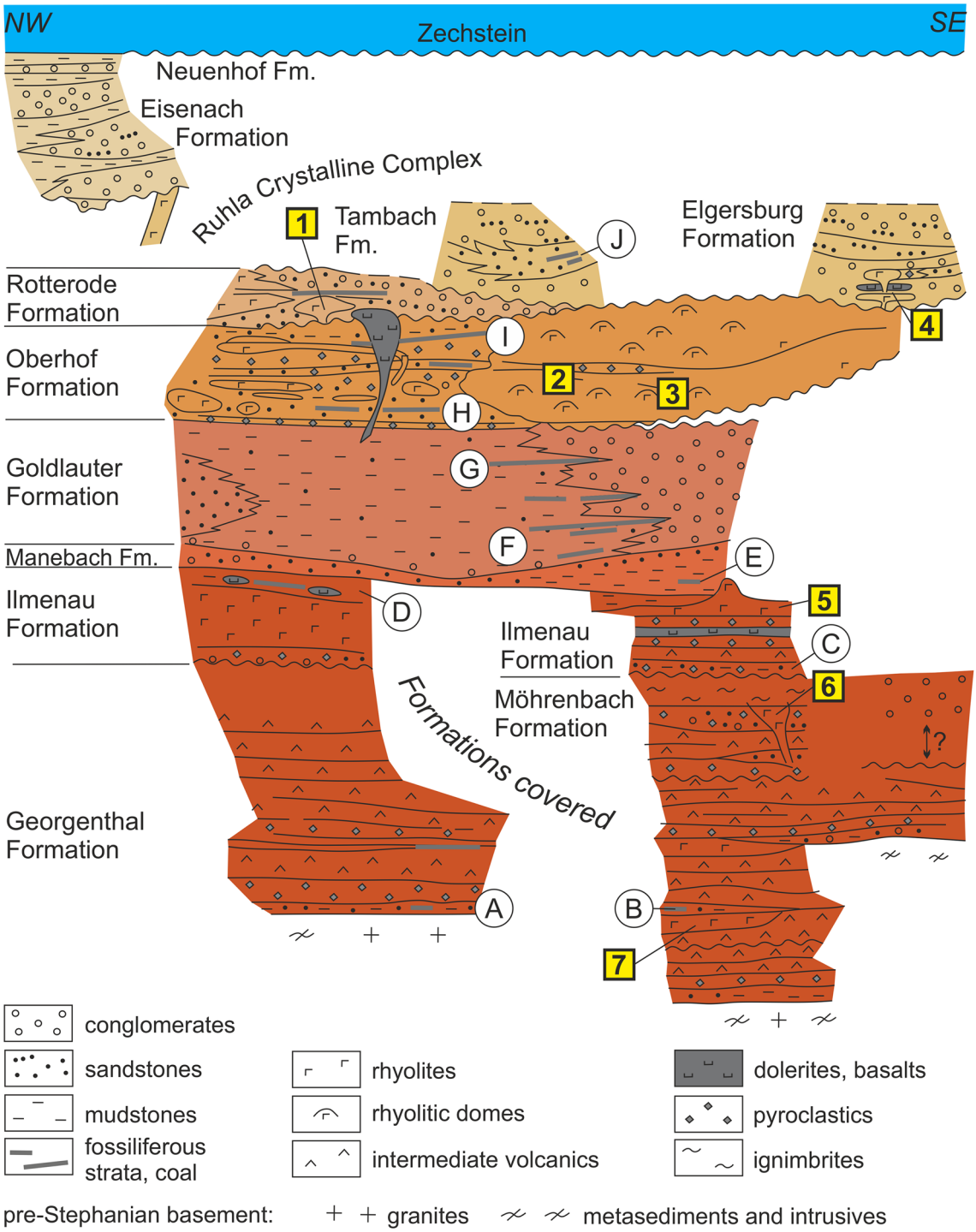

Fig. 2 Lithostratigraphic subdivision of the Carboniferous–Permian sediments of the Thuringian Forest Basin, presented as a schematic NW–SE cross–section. Circled letters label biostratigraphically important fossiliferous horizons: A—Öhrenkammer horizon (Georgenthal Fm.), B—Ilmtal horizon (Möhrenbach Fm.), C—Lindenberg horizon (base of Ilmenau Fm.), D—Sembachtal horizon (top of Ilmenau Fm.), E—Manebach fossiliferous horizons (Manebach Fm.), F—Sperbersbach horizon (lower Goldlauter Fm.), G—Gottlob horizon (upper Goldlauter Fm.), H—Lochbrunnen horizon (lower Oberhof Fm.), I—Wintersbrunn horizon (upper Oberhof Fm.), J—Bromacker horizon (Tambach Fm.). Numbers in yellow boxes represent new sample locations for zircon U–Pb CA–ID–TIMS dating

resulted in deposition of granite-derived sands and gravels (Thomson and Zeh 2000; Andreas and Lützner, 2009).

The Tambach Formation starts with coarse conglomerates that cover an eroded surface. The conglomerates grade upwards into red sandstones and mudstones that contain the youngest fossil beds of stratigraphic significance in the TFB. The fossil-bearing red beds at the Bromacker locality are famous for tetrapod footprints and skeletal remains of terrestrial amphibians and reptiles. Paleontological projects were performed by T. Martens in cooperation with experts from the USA (Martens 2001; Eberth et al. 2000 and others). The state of biostratigraphic correlation was summarized by Schneider et al. (2020). They consider for the Bromacker Horizon an Artinskian age, which is not proven by radioisotopic studies. Volcanic rocks are missing in the Tambach Formation; volcaniclastic rocks are also presently unknown.

The Eisenach Formation only occurs on the western flank of the Ruhla Crystalline Complex and the adjacent Werra basin. Along the basin fringes, marginal alluvial fans are interfingered with sandy mudstones.

The Neuenhof Formation is the uppermost Permian formation of continental red beds. It consists of a 5–10 m thin-bedded alternation with fine gravels, sandstones, and siltstones of a mainly fluvial environment. Locally intercalated cross-bedded sandstones are probably of aeolian origin. At the top, the red-colored sandstones gradually pass over into gray sediments that were reworked by the invading Zechstein Sea. A scarce settling with brachiopods has been proven in places. The Kupferschiefer black shale follows with a sharp boundary.

Magnetostratigraphically, all formations of the TFB, including the Eisenach Formation, belong to the Kiaman Reversed Superchron. Only the red beds of the Neuenhof Formation proved to be part of the Permian–Triassic Mixed Superchron (Isozaki 2009; Menning et al. 1988). Thus, the Illawarra Reversal (266.66 ± 0.76 Ma, Hounslow and Balabanov 2018) took place during a long hiatus (break of sedimentation, gap due to onlapping cover on morphology, and/or erosion). Nevertheless, the Neuenhof Formation has the appearance of the Rotliegend facies (Lützner et al. 2012), which is directly covered by the basal conglomerate and black shale (Kupferschiefer) of the Zechstein sea.

Samples and methods

Samples

We aimed to sample the whole Stephanian and early Permian sequence of the TFB by sampling various rhyolitic and rhyodacitic volcanic rocks (Figs. 1b, 2). From each formation, one or two samples were collected (Table 1). We preferred to sample acidic rocks with medium- to large-sized phenocrysts of quartz and feldspar because these rocks generally yielded sufficient zircon crystals. We briefly comment on the sample sites in the lithostratigraphic order (Fig. 2).

In the lowest section, rhyolites from the Möhrenbach and the Ilmenau Formations of the Southeastern TFB region were sampled. Samples were taken from two rhyolite outcrops within the Möhrenbach Formation: (i) from road cuts near Stützerbach (sample 7) and (ii) from the quarry at the Hundskopf hillside (sample 6). According to several authors (Andreas et al. 1974; Michael 1972; Lützner et al. 2012), the Stützerbach Rhyolite is situated in the middle section of the Möhrenbach Formation and thus has a somewhat lower position than the Hundskopf Rhyolite. The latter is considered to be a part of the Kienberg Rhyolite that occurs as a dissipated system of dykes, sill-like bodies, vent fillings and lava sheets. Both samples are good representatives of the Möhrenbach Formation.

The Ilmenau Formation (occurring above the Möhrenbach Formation) contains the Kickelhahn Rhyolite that typically has plenty of medium-sized quartz and feldspar phenocrysts and is well exposed at the type locality "High Hill Kickelhahn" near Ilmenau where sample 5 was taken. This formation is associated with thick pyroclastics.

The predominantly sedimentary Manebach and Goldlauter Formations were not sampled because these units lack extrusive volcanic rocks.

Extensive magmatic activity (rhyolites, rhyodacites, felsic intrusions, and various pyroclastic deposits) occurred in the Oberhof Formation. Two localities in the uppermost lava flow of the "Older Rhyolite Series" were selected near Luisenthal to sample a representative rhyolite in the middle section of the Oberhof Formation (based on the revised Geological Map; Enderlein and Ziegenhardt 1975; scale of 1: 25,000). Sample 2 was taken from the Klotzegrund valley and sample 3 from outcrops at the mouth of the Lehmgrund valley. Both samples represent different parts of a uniform rhyolite body.

The Rotterode Formation comprises two fault-bound rhyolite bodies that did not contain zircon. In addition, several rhyolite dykes penetrate the red beds of the Rotterode Formation. They have been mapped in detail by Patzelt (1966) and were adopted in a revised map of the Rotterode Formation by Andreas and Lützner (2009). We sampled one of the rhyolite dykes in an outcrop in the village Struth-Helmershof (sample 1). It should indicate the median or minimum age of the Rotterode Formation.

The red beds overlying the Rotterode Formation, i.e., the Tambach and Eisenach Formations, do not contain volcanic rocks. Only the Elgersburg Formation**,** which is considered as an equivalent of the Tambach Formation, contains two rhyolite bodies and a basaltic layer in the lower part (Schwalbenstein Conglomerate Member). The Elgersburg Rhyolite represents the uppermost volcanic rock in the

Table 1 List of samples

Sample no.	Location	GK25	Easting [m]	Northing [m]	Longitude [°E]	Latitude [°N]	Formation	Rock type
1	Struth-Helmershof, outcrops „Kronstein“ near cemetery	Blatt 5229 Tambach-Dietharz	4,394,900	5,624,700	50.74828	10.50931	Rotterode Formation	Komberg Rhyolite, dyke, intruded into sediments of the Rotterode Formation
2	Southeast of Luisenthal, Siegelgrund, right side of valley, at mouth of Klotzegrund valley	Blatt 5230 Oberhof	4,410,800	5,626,150	50.76397	10.73419	Oberhof Formation	„Zone der Älteren Porphyre, 6. Erguss“ (zone of older porphyries, 6th extrusion), according to mapping of Enderlein and Ziegenhardt (1975) a rhyolite sheet
3	Luisenthal, at the end of Lehmgrund, outcrop below Gothaer Hütte (Gotha Cabin)	Blatt 5230 Oberhof	4,409,950	5,628,600	50.78586	10.72155	Oberhof Formation	„Zone der Älteren Porphyre, 6. Erguss“ (zone of older porphyries, 6th extrusion), according to mapping of Enderlein and Ziegenhardt (1975) a rhyolite sheet
4	Kohltal, footpath to Wolfstein summit, lowest part of trail	Blatt 5331 Ilmenau	4,419,070	5,618,430	50.69580	10.85308	Supposed to be Elgersburg Formation	Rhyolite with large pale pink feldspars
5	Forest track at western flank of the Kleiner Herrmannstein	Blatt 5331 Ilmenau	4,419,800	5,616,020	50.67424	10.86393	Ilmenau Formation	Kickelhahn-Porphyry, light grey porphyric rhyolite
6	Quarry at Großer Hunds kopf, at the road from Allzunah to the Dreiherrenstein and to Neustadt a.R	Blatt 5331 Ilmenau	4,420,280	5,608,600	50.60762	10.87232	Möhrenbach Formation	Upper section, part of Öhrenstock-Schichten Kienberg Rhyolite (quartz poor to quartz free); Michael (1972) mapped this as a subvolcanic intrusion, time equivalent to the widely exposed Kienberg Rhyolite
7	Quarry at the road from Gasthof Auerhahn (inn) to Ilmenau, between Hinterer Erbskopf and Hohe Tanne	Blatt 5331 Ilmenau	4,420,830	5,612,500	50.64274	10.87925	Möhrenbach Formation, lower to middle section	Stützerbach Rhyolite, quartz poor to quartz free

Coordinates are given as Gauss–Krueger (Zone 4) for maximum precision and decimal degrees (WGS84) for international comparability. GK is the 1: 25,000 Geological Map of Thuringia

TFB. Unfortunately, separated zircons from this rhyolite had xenomorphic forms; idiomorphic grains were lacking. Therefore, we excluded this sample from dating and instead used the Wolfstein Rhyolite, which appears near the base of Elgersburg conglomerates (No. 4). It was first described as "Preußenshöhe Porphyr" by Zimmermann (in Loretz et al. 1908, p. 122) and Deubel (1960, p. 429). The Wolfstein Rhyolite is characterized by medium to large phenocrysts of quartz and feldspar and contains idiomorphic zircon crystals suitable for high-precision dating.

Methods

Recent development in ID-TIMS dating substantially reduced the analytical error of zircon dating, especially through the application of chemical abrasion (CA) on single zircon grains prior to their analysis. It was demonstrated in several studies that this pre-treatment considerably reduces Pb loss that—if not detected—would result in exceedingly young ages (Mattinson 2005; Schaltegger et al. 2015; Tichomirowa et al. 2019). In addition, due to efforts of the EARTHTIME initiative (http://www.earthtimetestsite.com/), the inter-laboratory bias of zircon ages has been reduced to 0.1% through the use of precisely and accurately calibrated tracers (Condon et al. 2015) and the standardization of raw data correction by the development and supply of open source programs (McLean et al. 2015). As a result, the accuracy and external reproducibility of zircon ages from participating laboratories can be ≤ 0.1% and can be proved by their reported international zircon standard ages. Consequently, the CA–ID–TIMS method has the ability to produce the most precise and accurate ages (Schaltegger et al. 2015).

U–Pb CA–ID–TIMS dating was performed in the TIMS lab at the TU Bergakademie Freiberg (Germany). Selected zircon grains with the most idiomorphic forms (ca. 15–30 per sample) were annealed for 72–96 h at 850 °C and subsequently chemically abraded for 12–15 h at 180 °C with concentrated HF and HNO_3. This procedure dissolves crystal domains with the most intense radiation damage, which are suspected to have experienced post-crystallization lead loss (Mattinson 2005). After this chemical leaching procedure, single idiomorphic grains are transformed into fragments that represent those zircon parts with the lowest uranium content (Mattinson 2005). Afterwards, the acid, together with dissolved zircon material, was completely pipetted out. 3.5 N HNO_3 was added to the remaining zircon fragments, and the mixture was left for 30 min at 50 °C to remove surface lead. Several cleaning cycles with water, combined with repeated ultrasonic treatment were conducted before single zircon fragments were selected for further processing.

Single zircon fragments were washed with 3 N HNO_3 and transferred into cleaned microcapsules with a small drop of this fluid and 3 drops of concentrated HF. Samples were spiked with 6–10 mg of a ^{205}Pb–^{233}U–^{235}U tracer solution (ET535 at TU Bergakademie Freiberg; Condon et al. 2015). For final dissolution, the microcapsules were placed in Parr vessels and heated to 200° C for 48 h followed by drying at 130 °C and then re-dissolution in 6 N HCl for 24 h at 200 °C to transfer them into chlorides. After repeated drying, the samples were dissolved in 10 drops (ca. 50–60 mg) of 3.1 N HNO_3 and transferred into 50 µl micro-columns for column chemistry. U and Pb were separated from the rest of the sample by anion exchange chromatography (AG 1-X8, 200–400 mesh) using HCl and H_2O. The U- and Pb-containing fraction was loaded on degassed rhenium filaments with a drop of silica gel and measured with a Finnigan Mass Spectrometer MAT 262 using a secondary electron multiplier (SEM). The common Pb was corrected using the model of Stacey and Kramers (1975) instead of applying a specific lab blank value because this correction resulted in the most concordant values for reference materials (two international standards—see below).

Ages of two international zircon standards (Temora 2, 91500) were acquired contemporaneously with those of the Thuringian Forest volcanic rocks to ensure their accuracy. Similar to the samples, both standards were pre-treated with chemical abrasion (CA) to get comparable results. Data are given as $^{206}Pb/^{238}U$ age-ranked plots in Fig. 3. The Temora 2 standard has an accepted age of 416.8 ± 0.3 Ma (Black et al. 2003). The majority of our single grain ages have a spread of < ± 0.3% with a few slightly older ages (Table 2, Fig. 3). We obtained a weighted mean age of 417.34 ± 0.28/0.33/0.56 Ma for this standard. The standard 91500 was dated at 1062.4 ± 0.4 Ma (Wiedenbeck et al. 1995) and 1063.6 ± 0.3 Ma (Schoene et al. 2006). In our data, a few ages are slightly (< 1%) younger than the main age cluster, indicating the presence of small lead loss despite CA pre-treatment (Table 2). The remaining data used for the weighted mean age calculation have a spread of < 0.3% and yielded a weighted mean age of 1064.6 ± 0.55/0.60/1.30 Ma (Fig. 3). Altogether, our results are within 0.1% of the accepted values, assuring the accuracy of our CA–ID–TIMS ages at the 0.1% level.

Results

The U–Pb isotopic results of seven samples are given in Table 2 and presented in Fig. 4 as $^{206}Pb/^{238}U$ age-ranked plots for each individual sample. Eight to fifteen grains were analyzed for each sample. Mean sample ages were calculated from age clusters that are interpreted as crystallization ages. The error of weighted mean ages is given as ± *x*/*y*/*z*, where *x* is the internal 2σ measurement error, *y* is the internal 2σ error plus tracer calibration uncertainty, and *z* additionally

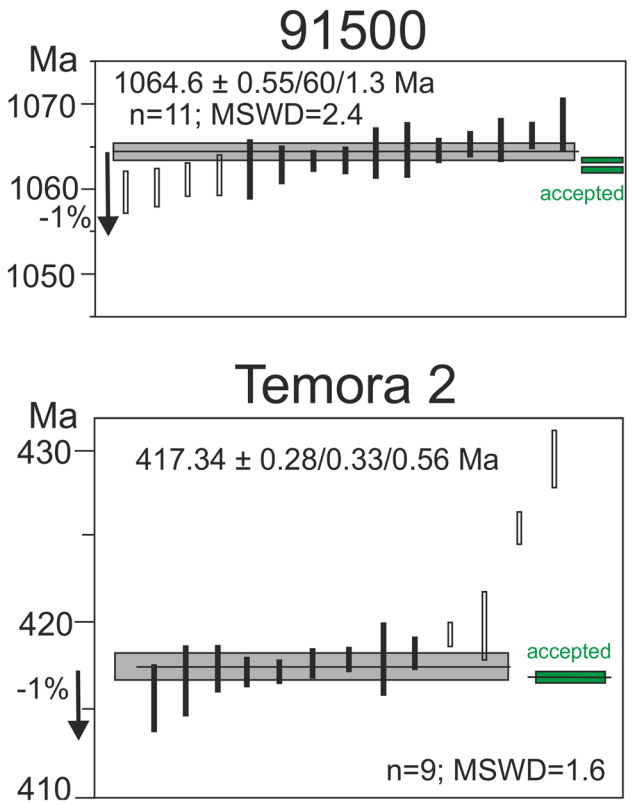

Fig. 3 $^{206}Pb/^{238}U$ ages of two international standards obtained by CA–ID–TIMS. Single ages are shown by bars representing 2σ errors (including analytical, tracer, and decay constant uncertainties); unfilled bars are considered outliers. All uncertainties associated with weighted mean $^{206}Pb/^{238}U$ ages are reported at the 95% confidence level and given as ± *x*/*y*/z, with *x* as analytical uncertainty, *y* including tracer calibration uncertainty, and *z* including ^{238}U decay constant uncertainty. The accepted mean ages, together with their 2σ uncertainties for these standards (see text for values) are given in green for comparison

includes the decay constant uncertainty (Schoene et al. 2006).

Nine zircons were dated from sample 1. The youngest age was discarded and interpreted as slight lead loss because of its offset from the remaining eight results. The other eight analyses yielded ages from 295.7 ± 0.2 Ma to 297.6 ± 0.9 Ma. The youngest three of these eight dates define a cluster of identical ages with a weighted mean age of 295.8 ± 0.1/0.2/0.4 Ma [mean square of weighted deviates (MSWD) = 0.1], which we interpret as the crystallization age. The five remaining dates show a slight increase from 296.3 ± 1.5 to 297.6 ± 0.9 Ma. These deviating ages are interpreted as zircons incorporated during intrusion from slightly older magma batches (antecrystic grains, Miller et al. 2007).

Analysis of six individual zircons from sample 2 yielded a statistically significant cluster with a weighted mean age of 296.8 ± 0.2/0.2/0.4 Ma (MSWD = 0.8). Two slightly older ages and one slightly younger age deviate from this cluster and have been discarded from the mean age calculation and are interpreted as antecrystic grains and grains affected by lead loss, respectively.

The weighted mean age of sample 3 was calculated from the youngest age cluster of three zircons yielding 296.9 ± 0.1/0.2/0.4 Ma (MSWD = 0.9, $n = 3$). Four grains are distinctly older, varying from 297.1 ± 0.3 Ma to 301.2 ± 1.2 Ma. These ages do not overlap with the calculated mean age and are interpreted as antecrystic (Miller et al. 2007) and/or inherited ages.

Ten single zircon grains were analyzed from sample 4. Three of them are more than 5 Ma older than the rest and are interpreted as inherited grains. Four of the remaining dates show a tendency towards younger ages, while the other three grains define an age cluster at 299.4 ± 0.3/0.3/0.5 Ma (MSWD = 1.3), interpreted as the crystallization age of this sample. If this interpretation is valid, severe lead loss has to be assumed for the remaining four grains (the youngest date results in 296.5 ± 0.4 Ma, which is 1% below the defined mean age). Therefore, lead loss is most pronounced in zircons from sample 4 but also present in zircons from samples 1, 2, 5, 6, and 7.

The analysis of 15 zircon grains from sample 5 yielded ages that range from 298.4 ± 0.2 Ma to 302.8 ± 0.1 Ma, with one inherited age at 319.3 ± 0.2 Ma. Three other grains are significantly older than the majority of ages and are interpreted as antecrystic zircons. The remaining eleven zircons reveal a much smaller scatter from 298.4 ± 0.2 Ma to 299.3 ± 0.1 Ma. We interpret the younger dates as affected by lead loss and calculated a weighted mean age of 299.3 ± 0.1/0.1/0.3 Ma (MSWD = 1.2) using the five oldest grains from this population.

Nine zircon grains were dated from sample 6. The statistically significant age cluster includes seven single grain ages and yields a weighted mean age of 300.0 ± 0.3/0.3/0.5 Ma (MSWD = 0.9). One age is significantly younger than this cluster and is interpreted as having been affected by lead loss; another age is significantly older and is interpreted as an antecrystic grain.

Ten zircon grains were analyzed from sample 7 and show ages from 298.0 ± 0.6 Ma to 299.9 ± 0.7 Ma. The youngest ages are not identical but show a tendency toward lower ages that is interpreted as having been affected by lead loss. A well-defined age cluster is formed by the four oldest grains of this sample at 299.7 ± 0.3/0.3/0.4 Ma (MSWD = 0.2).

Table 2 U–Pb CA–ID–TIMS analyses of standard and sample zircons; data used for $^{206}Pb/^{238}U$-weighted mean age calculations are given in bold

Fraction and sample	Dates (Ma)								Composition			Isotope ratios						
	$^{206}Pb/^{238}U$	±2σ	$^{207}Pb/^{235}U$	±2σ	$^{207}Pb/^{206}Pb$	±2σ	Corr. Coeff	%disc	Pb* [pg]	Pb_c [pg]	Pb*/Pb_c	$^{206}Pb/^{204}Pb$	$^{206}Pb/^{238}U$	±2σ	$^{207}Pb/^{235}U$	±2σ	$^{207}Pb/^{206}Pb$	±2σ
	a	(absolute)	a	(absolute)	a	(absolute)		b	c	d	e	f	g	(%)	g	(%)	g	(%)
91500																		
91500–1	1059.6	2.7	1065.5	19.1	1064	53	0.96	0.38	13.4	3.5	3.81	258	0.1799	0.27	1.8558	2.90	0.0748	2.63
91500–2	1060.1	2.4	1054.3	16.1	1045	45	0.90	0.26	35.8	8.0	4.49	302	0.1785	0.25	1.8246	2.46	0.0741	2.23
91500–3	1061.1	2.0	1056.3	4.0	1047	11	0.58	1.35	76.7	7.0	11.0	697	0.1789	0.18	1.8300	0.61	0.0742	0.52
91500–4	1061.9	1.8	1062.4	11.8	1067	33	0.88	1.26	22.1	3.6	6.17	406	0.1788	0.19	1.8472	1.79	0.0749	1.63
91500–5	**1062.3**	**3.4**	**1060.6**	**23.6**	**1063**	**66**	**0.93**	**0.03**	**10.9**	**3.5**	**3.07**	**212**	**0.1787**	**0.35**	**1.8421**	**3.58**	**0.0748**	**3.26**
91500–6	**1063.0**	**2.1**	**1055.6**	**9.2**	**1042**	**26**	**0.66**	**2.26**	**77.3**	**9.4**	**8.19**	**537**	**0.1791**	**0.21**	**1.8281**	**1.40**	**0.0740**	**1.27**
91500–7	**1063.3**	**1.1**	**1063.8**	**6.9**	**1067**	**19**	**0.84**	**0.33**	**69.5**	**6.5**	**10.6**	**685**	**0.1791**	**0.12**	**1.8510**	**1.05**	**0.0749**	**0.95**
91500–8	**1063.5**	**1.4**	**1059.9**	**3.2**	**1056**	**9**	**0.66**	**3.26**	**59.6**	**6.1**	**9.71**	**632**	**0.1791**	**0.09**	**1.8402**	**0.48**	**0.0745**	**0.43**
91500–9	**1064.5**	**2.9**	**1059.2**	**3.5**	**1052**	**10**	**0.53**	**1.14**	**59.4**	**6.2**	**9.51**	**619**	**0.1792**	**0.15**	**1.8382**	**0.54**	**0.0744**	**0.48**
91500–10	**1064.6**	**2.9**	**1064.6**	**3.6**	**1072**	**10**	**0.58**	**4.26**	**55.4**	**7.8**	**7.06**	**464**	**0.1789**	**0.14**	**1.8533**	**0.54**	**0.0751**	**0.48**
91500–11	**1064.9**	**1.2**	**1064.9**	**5.2**	**1066**	**14**	**0.67**	**0.14**	**109**	**7.6**	**14.3**	**920**	**0.1795**	**0.13**	**1.8541**	**0.79**	**0.0749**	**0.71**
91500–12	**1065.3**	**1.2**	**1061.3**	**1.0**	**1055**	**2**	**0.86**	**5.26**	**278**	**7.7**	**36.2**	**2299**	**0.1795**	**0.08**	**1.8439**	**0.15**	**0.0745**	**0.09**
91500–13	**1065.8**	**2.4**	**1064.5**	**15.3**	**1064**	**42**	**0.87**	**0.16**	**57.2**	**12**	**4.74**	**318**	**0.1796**	**0.25**	**1.8529**	**2.31**	**0.0748**	**2.10**
91500–14	**1066.2**	**1.4**	**1064.9**	**6.4**	**1064**	**18**	**0.71**	**6.26**	**45.5**	**3.9**	**11.6**	**749**	**0.1797**	**0.14**	**1.8542**	**0.97**	**0.0749**	**0.87**
91500–15	**1067.6**	**2.9**	**1065.8**	**21.6**	**1065**	**60**	**0.97**	**0.24**	**41.4**	**12**	**3.37**	**231**	**0.1799**	**0.30**	**1.8567**	**3.27**	**0.0749**	**2.97**
Temora2																		
Tem-1	**415.5**	**1.9**	**414.3**	**24.8**	**412**	**152**	**0.98**	**0.73**	**6.64**	**3.3**	**2.03**	**149**	**0.0664**	**0.49**	**0.5039**	**7.28**	**0.0550**	**6.80**
Tem-2	**416.5**	**1.9**	**416.7**	**3.1**	**419**	**17**	**0.55**	**0.64**	**185**	**9.9**	**18.6**	**1183**	**0.0667**	**0.40**	**0.5074**	**0.92**	**0.0552**	**0.78**
Tem-3	**416.8**	**0.9**	**418.3**	**11.0**	**429**	**67**	**0.93**	**2.86**	**15.6**	**3.4**	**4.55**	**302**	**0.0667**	**0.23**	**0.5098**	**3.20**	**0.0554**	**2.99**
Tem-4	**417.1**	**0.8**	**415.9**	**1.9**	**409**	**11**	**0.60**	**1.85**	**71.6**	**6.8**	**10.5**	**666**	**0.0668**	**0.10**	**0.5062**	**0.55**	**0.0549**	**0.49**
Tem-5	**417.2**	**0.6**	**417.9**	**5.9**	**423**	**36**	**0.86**	**1.48**	**32.8**	**3.8**	**8.66**	**562**	**0.0668**	**0.14**	**0.5091**	**1.74**	**0.0553**	**1.62**
Tem-6	**417.4**	**0.6**	**413.3**	**2.2**	**396**	**13**	**0.64**	**5.54**	**60.8**	**7.7**	**7.89**	**516**	**0.0667**	**0.09**	**0.5024**	**0.64**	**0.0546**	**0.59**
Tem-7	**417.8**	**0.7**	**414.3**	**2.1**	**401**	**13**	**0.65**	**4.09**	**62.6**	**11**	**5.96**	**400**	**0.0668**	**0.08**	**0.5038**	**0.63**	**0.0547**	**0.57**
Tem-8	**417.8**	**2.1**	**423.4**	**23.2**	**457**	**139**	**0.81**	**8.58**	**12.3**	**5.4**	**2.27**	**158**	**0.0669**	**0.58**	**0.5174**	**6.71**	**0.0561**	**6.25**
Tem-9	**418.2**	**0.9**	**418.6**	**6.3**	**423**	**38**	**0.76**	**1.03**	**31.3**	**5.9**	**5.32**	**350**	**0.0670**	**0.17**	**0.5102**	**1.83**	**0.0553**	**1.71**
Tem-10	419.3	0.6	417.8	7.9	412	48	0.96	1.86	20.0	3.1	6.46	430	0.0671	0.16	0.5090	2.29	0.0550	2.14
Tem-11	419.7	1.9	417.5	18.8	409	115	0.83	2.65	12.6	4.6	2.76	192	0.0672	0.45	0.5086	5.49	0.0549	5.13

Table 2 (continued)

Fraction and sample	Dates (Ma)								Composition			Isotope ratios						
	$^{206}Pb/^{238}U$	±2σ	$^{207}Pb/^{235}U$	±2σ	$^{207}Pb/^{206}Pb$	±2σ	Corr. Coeff	%disc	Pb* [pg]	Pb_c [pg]	Pb*/Pb_c	$^{206}Pb/^{204}Pb$	$^{206}Pb/^{238}U$	±2σ	$^{207}Pb/^{235}U$	±2σ	$^{207}Pb/^{206}Pb$	±2σ
	a	(absolute)	a	(absolute)	a	(absolute)		b	c	d	e	f	g	(%)	g	(%)	g	(%)
Tem-12	425.3	0.9	422.0	11.0	407	67	0.92	4.60	15.8	3.4	4.67	317	0.0681	0.23	0.5153	3.19	0.0549	2.97
Tem-13	429.5	1.8	422.2	22.8	388	139	0.96	10.8	8.40	3.7	2.24	162	0.0687	0.45	0.5156	6.61	0.0544	6.18
Sample 1																		
1-1	295.0	0.1	296.0	0.5	304	5	0.25	2.88	94.0	1.0	94.7	5803	0.0468	0.04	0.3385	0.21	0.0524	0.20
1-2	297.6	0.9	297.7	1.3	299	8	0.69	0.43	81.3	1.2	66.4	4083	0.0472	0.32	0.3407	0.50	0.0523	0.36
1-3	296.9	0.3	297.2	1.8	299	16	0.15	0.83	53.1	1.9	28.0	1717	0.0471	0.11	0.3401	0.70	0.0523	0.69
1-4	296.4	0.4	297.3	0.6	304	3	0.88	2.57	208	1.3	162	9895	0.0471	0.14	0.3401	0.25	0.0524	0.14
1-5	**295.7**	**0.2**	**296.2**	**1.1**	**300**	**10**	**0.19**	**1.34**	**38.6**	**0.9**	**44.2**	**2734**	**0.0469**	**0.06**	**0.3387**	**0.44**	**0.0523**	**0.44**
1-6	**295.8**	**0.2**	**297.3**	**0.5**	**309**	**4**	**0.40**	**4.42**	**85.3**	**0.7**	**120**	**7297**	**0.0470**	**0.06**	**0.3402**	**0.18**	**0.0526**	**0.16**
1-7	296.5	0.2	297.4	1.3	305	11	0.17	2.83	28.9	0.7	38.7	2347	0.0471	0.07	0.3403	0.51	0.0525	0.50
1-8	**296.3**	**1.5**	**300.4**	**4.4**	**333**	**36**	**0.31**	**11.1**	**84.8**	**7.3**	**11.6**	**725**	**0.0470**	**0.52**	**0.3443**	**1.67**	**0.0531**	**1.59**
1-9	297.3	1.4	308.3	7.5	392	63	0.16	24.2	37.3	6.0	6.23	392	0.0472	0.48	0.3548	2.83	0.0545	2.79
Sample 2																		
2-1	296.0	0.3	299.6	1.6	328	14	0.15	9.65	198	6.7	29.6	1855	0.0470	0.10	0.3432	0.62	0.0530	0.61
2-2	**296.8**	**0.3**	**300.0**	**2.9**	**326**	**25**	**0.09**	**8.88**	**113**	**6.8**	**16.7**	**1033**	**0.0471**	**0.11**	**0.3438**	**1.12**	**0.0529**	**1.12**
2-3	297.4	0.4	299.7	1.7	317	15	0.18	6.17	180	6.4	28.3	1734	0.0472	0.12	0.3433	0.65	0.0527	0.64
2-4	297.3	1.1	299.8	6.9	319	60	0.13	6.94	104	15	7.08	448	0.0472	0.37	0.3435	2.67	0.0528	2.65
2-5	**296.6**	**0.7**	**298.6**	**3.3**	**314**	**29**	**0.18**	**5.64**	**195**	**13**	**14.9**	**920**	**0.0471**	**0.25**	**0.3418**	**1.29**	**0.0527**	**1.27**
2-6	**296.4**	**0.6**	**298.8**	**2.6**	**317**	**22**	**0.21**	**6.62**	**135**	**7.4**	**18.3**	**1174**	**0.0470**	**0.21**	**0.3421**	**0.99**	**0.0527**	**0.97**
2-7	**296.7**	**0.3**	**300.4**	**3.4**	**329**	**30**	**0.08**	**9.85**	**75.8**	**5.3**	**14.4**	**886**	**0.0471**	**0.11**	**0.3442**	**1.31**	**0.0530**	**1.30**
2-8	**297.0**	**0.4**	**300.4**	**4.1**	**327**	**35**	**0.08**	**9.15**	**67.3**	**5.7**	**11.8**	**743**	**0.0472**	**0.14**	**0.3443**	**1.57**	**0.0530**	**1.56**
2-9	**296.4**	**1.4**	**300.2**	**23.1**	**329**	**202**	**0.01**	**9.92**	**22.1**	**9.1**	**2.42**	**146**	**0.0471**	**0.48**	**0.3439**	**8.91**	**0.0530**	**8.92**
Sample 3																		
3-1	298.1	0.2	299.3	1.5	308	13	0.17	3.31	115	3.5	33.0	2039	0.0473	0.06	0.3428	0.58	0.0525	0.58
3-2	299.3	0.3	299.9	2.1	305	19	0.12	1.73	57.1	2.3	24.9	1440	0.0475	0.10	0.3436	0.82	0.0524	0.81
3-3	297.6	0.2	298.1	1.7	302	15	0.10	1.51	47.2	1.5	30.8	1819	0.0472	0.06	0.3413	0.65	0.0524	0.64
3-4	**297.1**	**0.3**	**298.1**	**0.4**	**306**	**3**	**0.59**	**3.05**	**307**	**1.9**	**165**	**9854**	**0.0472**	**0.09**	**0.3413**	**0.15**	**0.0525**	**0.12**
3-5	297.5	0.3	298.6	0.8	307	7	0.30	3.14	111	1.8	63.3	3772	0.0472	0.10	0.3419	0.33	0.0525	0.31
3-6	**296.9**	**0.1**	**298.1**	**0.4**	**307**	**4**	**0.34**	**3.32**	**97.5**	**0.8**	**116**	**7456**	**0.0471**	**0.05**	**0.3412**	**0.17**	**0.0525**	**0.16**
3-8	**297.6**	**2.4**	**297.0**	**4.1**	**292**	**32**	**0.50**	**1.86**	**114**	**9.4**	**12.2**	**784**	**0.0472**	**0.81**	**0.3397**	**1.61**	**0.0522**	**1.39**
3-9	301.2	1.2	301.8	8.3	306	72	0.11	1.72	73.5	13	5.82	377	0.0478	0.40	0.3461	3.18	0.0525	3.17

Table 2 (continued)

Fraction and sample	Dates (Ma)								Composition			Isotope ratios						
	$^{206}Pb/^{238}U$	±2σ	$^{207}Pb/^{235}U$	±2σ	$^{207}Pb/^{206}Pb$	±2σ	Corr. Coeff	%disc	Pb* [pg]	Pb_c [pg]	Pb*/Pb_c	$^{206}Pb/^{204}Pb$	$^{206}Pb/^{238}U$	±2σ	$^{207}Pb/^{235}U$	±2σ	$^{207}Pb/^{206}Pb$	±2σ
	a	(absolute)	a	(absolute)	a	(absolute)		b	c	d	e	f	g	(%)	g	(%)	g	(%)
Sample 4																		
4-1	**299.6**	**0.7**	**302.0**	**10.6**	**321**	**92**	**0.03**	**6.67**	**18.0**	**3.9**	**4.61**	**300**	**0.0476**	**0.23**	**0.3464**	**4.06**	**0.0528**	**4.07**
4-2	296.5	0.4	297.7	4.7	307	41	0.05	3.36	51.4	5.2	9.92	647	0.0471	0.13	0.3407	1.81	0.0525	1.80
4-3	296.6	0.5	299.1	6.8	319	60	0.02	7.01	29.4	4.1	7.16	452	0.0471	0.16	0.3426	2.62	0.0528	2.62
4-4	298.2	0.5	300.5	7.2	319	63	0.04	6.45	30.3	4.5	6.81	429	0.0473	0.17	0.3444	2.76	0.0528	2.76
4-5	306.0	1.3	304.9	20.8	297	180	0.03	3.13	8.03	3.4	2.35	166	0.0486	0.44	0.3502	7.89	0.0523	7.89
4-6	305.6	1.2	307.6	18.8	322	161	0.02	5.23	15.6	5.7	2.72	179	0.0486	0.39	0.3538	7.07	0.0529	7.08
4-7	**299.1**	**0.5**	**301.9**	**7.3**	**323**	**64**	**0.03**	**7.43**	**26.7**	**3.9**	**6.90**	**423**	**0.0475**	**0.17**	**0.3462**	**2.80**	**0.0529**	**2.80**
4-8	297.9	0.4	300.9	5.0	323	44	0.05	7.89	36.0	3.6	9.92	602	0.0473	0.14	0.3449	1.94	0.0529	1.93
4-9	**299.6**	**0.4**	**300.2**	**6.7**	**304**	**59**	**0.04**	**1.54**	**28.8**	**4.1**	**7.05**	**464**	**0.0476**	**0.15**	**0.3439**	**2.58**	**0.0524**	**2.58**
4-10	305.9	0.5	307.8	6.9	322	59	0.03	4.94	26.6	3.9	6.79	452	0.0486	0.16	0.3541	2.62	0.0528	2.62
Sample 5																		
5-1	298.9	0.1	299.0	0.4	300	3	0.49	0.33	89.2	0.5	169	10,120	0.0475	0.04	0.3425	0.15	0.0523	0.13
5-2	298.7	0.9	296.5	1.8	279	13	0.55	7.10	44.6	0.8	53.0	3139	0.0474	0.30	0.3391	0.69	0.0519	0.58
5-3	302.8	0.1	303.6	0.2	310	1	0.73	2.35	299	0.5	556	33,312	0.0481	0.04	0.3485	0.07	0.0526	0.05
5-4	**299.2**	**0.2**	**299.5**	**0.4**	**301**	**3**	**0.43**	**0.70**	**54.7**	**0.3**	**159**	**9285**	**0.0475**	**0.05**	**0.3430**	**0.16**	**0.0524**	**0.14**
5-5	**299.2**	**0.4**	**299.3**	**1.1**	**300**	**9**	**0.33**	**0.32**	**47.5**	**0.9**	**51.0**	**2938**	**0.0475**	**0.13**	**0.3428**	**0.44**	**0.0523**	**0.41**
5-6	**299.8**	**0.7**	**299.8**	**0.8**	**300**	**3**	**0.89**	**0.07**	**91.9**	**0.4**	**246**	**14,432**	**0.0476**	**0.25**	**0.3434**	**0.29**	**0.0523**	**0.13**
5-7	**299.2**	**0.2**	**299.7**	**0.5**	**304**	**4**	**0.35**	**1.50**	**124**	**1.1**	**118**	**7221**	**0.0475**	**0.05**	**0.3433**	**0.18**	**0.0524**	**0.16**
5-8	298.8	0.1	299.1	0.4	301	3	0.33	0.88	107	0.7	148	8911	0.0474	0.03	0.3426	0.14	0.0524	0.14
5-9	301.7	0.7	301.8	0.7	303	2	0.94	0.35	339	1.1	322	19,103	0.0479	0.25	0.3462	0.28	0.0524	0.10
5-10	319.3	0.2	314.7	0.8	281	7	0.22	13.8	107	1.6	66.7	3892	0.0508	0.06	0.3633	0.31	0.0519	0.30
5-11	298.4	0.2	298.4	0.9	299	8	0.25	0.09	98.7	1.7	57.4	3470	0.0474	0.07	0.3416	0.36	0.0523	0.34
5-12	298.9	0.2	299.4	1.1	304	9	0.28	1.54	128	2.6	49.2	2978	0.0475	0.07	0.3429	0.42	0.0524	0.41
5-13	300.1	0.2	300.7	1.3	306	11	0.27	1.95	30.5	0.7	43.0	2538	0.0476	0.06	0.3447	0.49	0.0525	0.48
5-14	298.8	0.1	299.4	0.8	304	7	0.20	1.57	116	1.7	68.2	4023	0.0474	0.05	0.3429	0.30	0.0524	0.30
5-15	**299.3**	**0.1**	**300.3**	**0.6**	**308**	**5**	**0.28**	**2.72**	**64.1**	**0.7**	**91.4**	**5296**	**0.0475**	**0.05**	**0.3441**	**0.24**	**0.0525**	**0.23**
Sample 6																		
6-1	**300.1**	**0.9**	**299.7**	**12.8**	**297**	**112**	**0.10**	**1.22**	**24.8**	**5.7**	**4.37**	**250**	**0.0477**	**0.32**	**0.3434**	**4.93**	**0.0523**	**4.90**
6-2	**300.2**	**1.2**	**305.0**	**18.7**	**342**	**161**	**0.04**	**12.2**	**17.2**	**5.4**	**3.19**	**177**	**0.0477**	**0.42**	**0.3504**	**7.10**	**0.0533**	**7.10**
6-3	301.5	0.7	304.6	8.2	328	70	0.05	8.19	22.9	3.5	6.63	382	0.0479	0.22	0.3499	3.10	0.0530	3.09
6-4	**299.7**	**0.6**	**301.9**	**9.1**	**319**	**79**	**0.03**	**6.02**	**24.2**	**4.0**	**6.12**	**344**	**0.0476**	**0.21**	**0.3463**	**3.48**	**0.0528**	**3.48**

Table 2 (continued)

Fraction and sample	Dates (Ma)								Composition			Isotope ratios						
	$^{206}Pb/^{238}U$	±2σ	$^{207}Pb/^{235}U$	±2σ	$^{207}Pb/^{206}Pb$	±2σ	Corr. Coeff	%disc	Pb* [pg]	Pb_c [pg]	Pb*/Pb_c	$^{206}Pb/^{204}Pb$	$^{206}Pb/^{238}U$	±2σ	$^{207}Pb/^{235}U$	±2σ	$^{207}Pb/^{206}Pb$	±2σ
	a	(absolute)	a	(absolute)	a	(absolute)		b	c	d	e	f	g	(%)	g	(%)	g	(%)
6-5	**299.9**	**0.7**	**300.1**	**9.5**	**302**	**83**	**0.08**	**0.69**	**18.4**	**3.2**	**5.74**	**326**	**0.0476**	**0.24**	**0.3439**	**3.66**	**0.0524**	**3.65**
6-6	295.3	0.7	298.3	9.7	321	85	0.03	8.12	24.4	4.1	5.97	321	0.0469	0.23	0.3415	3.75	0.0528	3.75
6-7	**300.0**	**0.4**	**302.3**	**5.0**	**320**	**44**	**0.06**	**6.36**	**36.6**	**3.3**	**11.1**	**607**	**0.0476**	**0.15**	**0.3468**	**1.93**	**0.0528**	1.92
6-8	**299.8**	**0.7**	**302.3**	**9.8**	**322**	**85**	**0.03**	**6.96**	**40.5**	**6.4**	**6.28**	**323**	**0.0476**	**0.22**	**0.3468**	**3.73**	**0.0528**	3.73
6-9	**300.4**	**0.6**	**301.2**	**4.7**	**307**	**41**	**0.11**	**2.18**	**38.4**	**3.2**	**11.9**	**643**	**0.0477**	**0.19**	**0.3453**	**1.81**	**0.0525**	1.80
Sample 7																		
7-2	298.0	0.6	301.0	7.0	324	61	0.05	8.03	47.0	5.9	7.92	441	0.0473	0.21	0.3450	2.68	0.0529	2.68
7-3	298.9	0.6	301.7	8.6	323	75	0.04	7.44	24.4	3.6	6.81	362	0.0475	0.20	0.3460	3.30	0.0529	3.30
7-4	298.9	0.4	301.2	4.1	319	36	0.08	6.44	49.5	3.4	14.5	741	0.0475	0.15	0.3453	1.57	0.0528	1.57
7-5	**299.7**	**0.6**	**302.6**	**8.7**	**325**	**75**	**0.03**	**7.86**	**24.3**	**3.4**	**7.18**	**357**	**0.0476**	**0.22**	**0.3472**	**3.31**	**0.0529**	**3.31**
7-6	**299.9**	**0.7**	**301.5**	**6.0**	**314**	**52**	**0.09**	**4.48**	**33.7**	**3.5**	**9.69**	**516**	**0.0476**	**0.22**	**0.3457**	**2.29**	**0.0527**	**2.28**
7-7	**299.6**	**0.5**	**301.6**	**4.8**	**317**	**42**	**0.11**	**5.53**	**43.7**	**3.9**	**11.2**	**629**	**0.0476**	**0.18**	**0.3458**	**1.84**	**0.0527**	**1.83**
7-8	299.5	0.4	301.8	4.6	320	40	0.08	6.45	38.2	3.2	12.0	656	0.0476	0.14	0.3462	1.76	0.0528	1.76
7-9	299.3	0.5	301.5	6.0	319	52	0.03	6.14	31.9	3.3	9.57	512	0.0475	0.16	0.3458	2.29	0.0528	2.29
7-10	298.9	0.4	302.5	4.6	331	40	0.05	9.66	40.6	3.2	12.7	656	0.0475	0.12	0.3471	1.78	0.0530	1.77
7-11	**299.7**	**0.5**	**302.3**	**6.9**	**322**	**60**	**0.03**	**6.96**	**26.2**	**3.3**	**7.96**	**451**	**0.0476**	**0.16**	**0.3468**	**2.63**	**0.0528**	**2.63**

a—Isotopic dates calculated using $\lambda_{238} = 1.55125E^{-10}$ (Jaffey et al. 1971) and $\lambda_{235} = 9.8485E^{-10}$ (Jaffey et al. 1971)

b—% discordance = 100 − (100 × ($^{206}Pb/^{238}U$ date)/($^{207}Pb/^{206}Pb$ date))

c—Total mass of radiogenic Pb

d—Total mass of common Pb

e—Ratio of radiogenic Pb (including ^{208}Pb) to common Pb

f—Measured ratio corrected for fractionation and spike contribution only

g—Measured ratios corrected for fractionation, tracer and blank

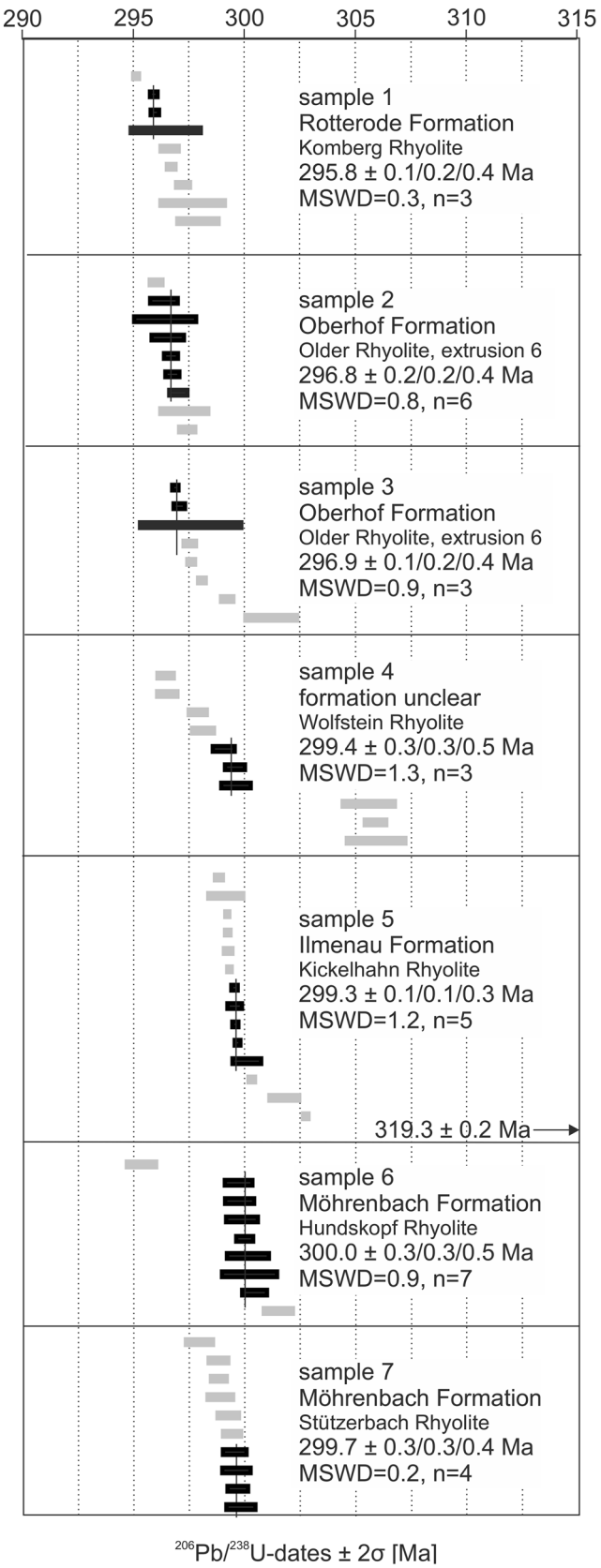

Fig. 4 New single grain zircon analyses and $^{206}Pb/^{238}U$-weighted ▶ mean ages for the Thuringian Forest Section. Each single zircon grain/fragment analysis including its 2σ uncertainty is represented by a horizontal bar. Grey bars are not included in the calculation of weighted mean ages. The weighted mean ages are shown by vertical lines. Uncertainty in the weighted mean ages are reported as *x*/*y*/*z*, where *x* is the internal 2σ measurement error, *y* is the internal 2σ error plus tracer calibration uncertainty, and *z* additionally includes the uncertainty of the decay constant (Schoene et al. 2006)

Discussion

New radiometric zircon ages

We discuss the results in stratigraphic order, first with regard to the lithostratigraphic subdivision of the TFB, then to the biostratigraphic aspects. In the following, we use the error expressed as z that also includes the error in tracer calibration and that of the decay constant (see above). This allows us to compare our ages to those obtained with other tracers and other dating systems.

Samples 7 and 6 yielded identical (within errors) $^{206}Pb/^{238}U$ mean ages (299.7 ± 0.4 Ma vs. 300.0 ± 0.5 Ma) representing the age of the Möhrenbach Formation. Considering the uncertain lithostratigraphic relation between the two sample sites (compare with Section "Geological setting"), the results of samples 7 and 6 clearly indicate an age in the range between 300.5 Ma and 299.3 Ma for the middle to upper part of the Möhrenbach Formation. Consequently, the Möhrenbach Formation was deposited during the latest Carboniferous, i.e., the Gzhelian (Standard Global Chronostratigraphic Scale) or Stephanian (West European regional scale).

Our new age of the Ilmenau Formation (sample 3) is the first precise depositional age for this unit. The sample dates the Kickelhahn Rhyolite near Manebach to 299.3 ± 0.3 Ma. This age overlaps with the recorded age of the Carboniferous–Permian boundary (298.90 ± 0.15 Ma; International Chronostratigraphic Chart 2019/05; the age was obtained by the same U–Pb CA–ID–TIMS method using the 535 spike; Ramezani et al. 2007). Thus, the age of the Kickelhahn Rhyolite provides important information for the stratigraphic position of the C–P boundary in the Thuringian Forest Basin, which has long been discussed as not exactly known.

After mapping the TFB on a scale of 1: 25,000, Beyschlag (1895: p. 599) concluded that "late" Carboniferous deposits are missing in the Thuringian Forest and that the entire sequence belongs to the Rotliegend (synonym for "Lower" Permian). Later, Gothan (1928) described from the basal, coal-seam-bearing sediments at the Öhrenkammer near Ruhla (letter A in Fig. 2) a peat-forming flora with Stephanian characteristic forms, which (supposedly) no longer occur in the Rotliegend. The Stephanian age of the Öhrenkammer and Ilmtal horizons (letters A and B, Fig. 2)

was also confirmed by the fauna of insects and amphibians (Schneider 1996; Schneider and Werneburg 2006, 2012). From then on, the C–P boundary was assumed to be undefined in the overlying volcanic sequence. Barthel and Rößler (2010) described plant remains from a silicified tuff horizon at the base of the Ilmenau Formation on the Lindenberg hill near Ilmenau (letter C in Fig. 2) as a typical Rotliegend flora. According to this assessment, the C–P boundary was "tentatively" assumed at the base of the Ilmenau Formation (Lützner et al. 2012; Gebhardt et al. 2018; Schneider et al. 2020).

The Kickelhahn Rhyolite (near Manebach village) is only covered by 10–15 m of tuffaceous conglomerates, above which the Manebach Formation begins with grey fluviatile sandstones. In the northwestern part of the Thuringian Forest, above an approx. 100 m thick rhyolite, 30 m of grey to black, fossil-rich lake sediments with tuff layers and subeffusive mafic rocks follow (formerly called "Melaphyr"). These rocks are covered by gray sandstones of the Manebach Formation. Considering the low thickness of post-rhyolitic volcanoclastic sedimentation, we estimate that the C–P boundary should be positioned approximately

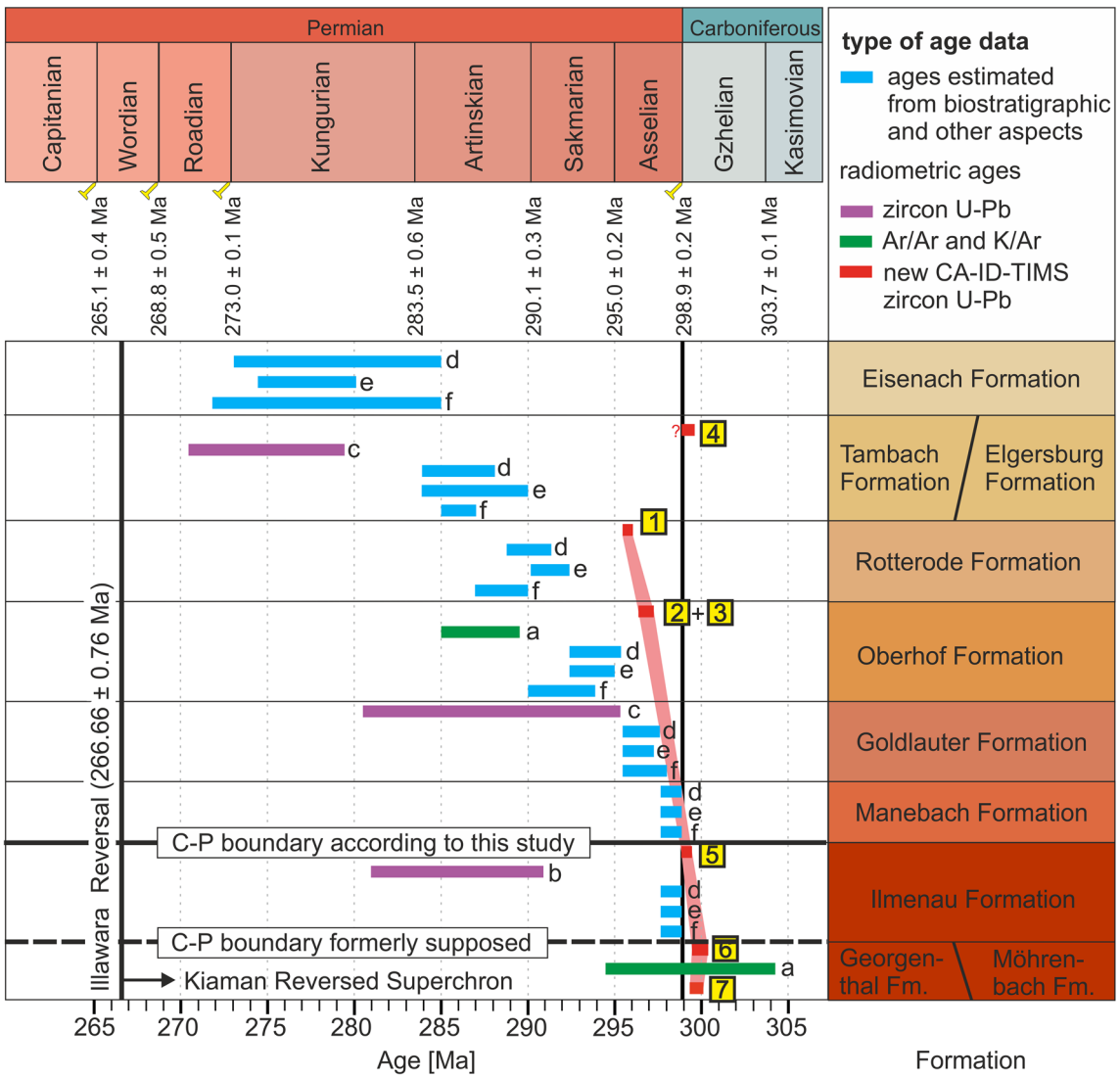

Fig. 5 Compilation of age data from the Rotliegend section of the Thuringian Forest. Radiometric age data are from **a** Goll and Lippolt (2001), **b** Zeh and Brätz (2000), **c** Lützner et al. (2007). The blue bars show the tentative assessment of the Thuringian Forest formations to the International Stratigraphic Chart 2019 after **d** Schneider and Werneburg (2012), **e** Menning et al. (2016; explanatory notes in Gebhardt et al. 2018) and **f** Schneider et al. (2020). Our new CA–ID–TIMS ages are shown in red. Numbers in yellow boxes are sample numbers for new zircon U–Pb CA–ID–TIMS dating. Obviously, most of the previous age data and assessments are remarkably younger than the new zircon ages

at the boundary between the Ilmenau and Manebach Formations (cp. Fig. 5).

The U–Pb zircon age of a silicified tuff layer from the middle part of the Manebach Formation was determined to be 297.8 ± 2.0 Ma by laser ICP–MS (Trümper et al. 2020). This finding fits well with the result of sample 5 (Fig. 6).

Our new data suggest an age difference of about 2.5 Myr between sample 5 und sample 3. During this time, the Manebach and Goldlauter Formations filled a pull-apart basin with paludal, lacustrine, fluvial, and alluvial sediments. The thickness of both formations is nearly 1000 m, i.e., the rate of subsidence (uncorrected) corresponds to about 400 m/Myr. Such subsidence rates are common in grabens/rift settings (e.g., Einsele 1992; Doglioni et al. 1998) and can reach extreme values in pull-apart basins like in the Ridge Basin in California (e.g., Yeats 1978: 2000 m/Myr).

Samples 3 and 2 reflect the culmination of the second volcanic phase within the TFB, which occurred in the range between 296 and 297 Ma. In future studies, it will be possible to better constrain the age of the Oberhof Formation by dating the rhyolites at the base (Heuberg- and Inselsberg Rhyolite) and the coarse crystalline Greifenberg rhyolite in dome structures near the upper boundary at the site of Großer Buchenberg near Tambach-Dietharz.

The age of the Komberg Rhyolite intrusion is provided by sample 1 and dates the red beds of the Rotterode Formation. As this formation clearly overlies the Oberhof Formation, the youngest zircon age of this sample (295.8 ± 0.4 Ma) is in agreement with the stratigraphy.

Sample 4 was dated with the idea of determining a representative age for the Elgersburg Formation. However, the obtained age is much older than expected; similar to that of the Möhrenbach Formation. The Wolfstein Rhyolite is directly bordered by the Schöffenhaus fault that dislocates the Elgersburg Formation against members of the Ilmenau Formation and the Oberhof or (in question) Rotterode Formations. Thus, we suggest that the Wolfstein Rhyolite could be interpreted as a small, tectonically uplifted block. Similar small uplifted blocks are well known from faults along the southwestern margin of the Thuringian Forest. The rock type of the Wolfstein Rhyolite with especially large phenocrysts of quartz and feldspar occurs within the Möhrenbach Formation as a widely ramified rhyolite dyke system. It has been described as Meyersgrund Rhyolite by Zimmermann (in Loretz et al. 1908: p. 100, 126), named after a tributary valley of the Ilm river.

In most occurrences of this Meyersgrund Rhyolite, the large quartz and feldspar phenocrysts are very fresh. In

Basins in Germany									Czech/Polish Basins[4, 5]		Basins in France[6]
Thuringian Forest Basin					SNB	HB	SB	DB	BF	ISB/RB	AB
lithostratigraphic units	fossil horizon (Fig. 2)	amphibian zonation[1, 2]	insect zonation[1, 2]	CA-ID-TIMS age[3] LA-ICP-MS age[7]							
Tambach Fm / Elgersburg Fm	J		(11)						<8> (11) Letovice Fm		
Rotterode Fm				295.8 ± 0.4 Ma							
Oberhof Fm	I	<7>		296.8 ± 0.4 Ma; 296.9 ± 0.4 Ma	<7> (10) Humberg h.	<7> Schöneck Fm		<7> Niederhäslich Fm, lm		<7> Olevětín Member, lm, ISB; 297.1 ± 0.3 Ma Broumov Fm; rhyolite ISB	
	H	<6>									
Goldlauter Fm	G	<5>									
	F	<5>	(8) (7)						(7) 298.9 ± 0.4 Ma Padochov Fm		
Manebach Fm	E		(6)	297.8 ± 2.0 Ma tuff layer							
Ilmenau Fm	D	<4>									<4> (7) from 298.0 ± 0.4 Ma Muse Fm to 298.9 ± 0.4 Ma
				299.3 ± 0.3 Ma							
	C										
Georgenthal Fm / Möhrenbach Fm				300.0 ± 0.5 Ma							
	A, B	<3>?			(5) Breitenbach Fm		<3> (5) Wettin Member			<3> Lině Fm, RB	
				299.7 ± 0.4 Ma							

Basins: SNB - Saar-Nahe-Basin, HB - Hessian Basin, SB - Saale Basin, DB - Döhlen Basin, BF - Boskovice Furrow, ISB - Intrasudetic Basin, RB - Roudnice Basin, AB - Autun Basin. Fm - Formation, h - horizon, lm - limestone.
Biostratigraphic zoning, amphibians: <3> *Apateon intermedius - Branchierpeton saalense*; <4> *Apateon dracyi - Melanerpeton sembachense;* <5> *Melanerpeton eisfeldi - Apateon flagrifer flagrifer - Branchierpeton reinholdi*; <6> *Apateon flagrifer oberhofensis - Melanerpeton arnhardti*; <7> *Melanerpeton pusillum - Melanerpeton gracile*; <8> *Discosauriscus austriacus*; insects: (5) *Sysciophlebia euglyptica - Sysciblatta dohrni*; (6) *Sysciophlebia ilfeldensis - Spiloblattina weissigensis*; (7) *Sysciophlebia balteata* H - *Spiloblattina homigtalensis*; (8) *Sysciophlebia balteata* G - *Sysciblattina sperbersbachensis*; (10) *Sysciophlebia* n. sp. B - *Spiloblattina odernheimensis;* (11) *Sysciblatta* n. sp. Form Obora - *Moravamylacris kukulovae*.
CA-ID-TIMS ages: All errors are given as z-values including uncertainties for tracer calibration and for the decay constant. In the TFB, all samples represent rhyolites.
References: 1 - Werneburg in Schneider et al. (2020); 2 - Schneider et al. (2020); 3 - this study; 4 - Opluštil et al. (2016); 5 - Opluštil et al. (2017); 6 - Pellenard et al. (2017); 7 - Trümper et al (2020).

Fig. 6 CA–ID–TIMS U–Pb zircon age data of the TFB and surrounding basins in relation to biostratigraphic zoning based on amphibians and insects

contrast, the Wolfstein Rhyolite is found in a highly altered state. In the small outcrop area, the rock is often so strongly weathered that the phenocrysts can only be recognized as hollow forms. It is possible that the fluid movements on the Schöffenhaus fault zone led to a particularly strong alteration. The result of sample 4 is also difficult to interpret due to the wide dispersion of the single grain ages and the low cluster density. For example, taking only the two youngest dates as clusters, the resulting age would be almost identical with sample 1, close to the expected age of the Elgersburg Formation.

The new zircon data for the profile of Carboniferous–Permian volcanic rocks in the TFB show older ages compared to the previously published age data (Fig. 5; data in summarized form in Lützner et al. 2012). This reflects the fact that the pre-treatment of the dated zircons by CA removed those components that suffered severe Pb loss. For most dated samples, the still-existing slight Pb loss resulted in few single ages that are 1–2 Ma younger than the calculated mean age (Fig. 4). Exceptions are sample 4 (which still has pronounced Pb loss; many single grain ages are up to 4 Ma younger) and one measurement of sample 6 (that is 5 Ma younger than the mean age). In general, the new zircon ages (single zircon ages as well as mean sample ages) show less age scatter than those of earlier publications. Consequently, the total duration of the volcanic activity in the TFB was considerably shorter. Whereas previously an age interval between 295 and 275 Ma was expected for the interval between the Möhrenbach Formation and the Elgersburg Formation (Lützner et al. 2007), our new data suggest a range between ca. 300 Ma for the Möhrenbach Formation and ca. 296 Ma for the Rotterode Formation. Even if the age of the youngest rhyolite (Elgersburg) has not yet been determined, the total duration of volcanic activity has to be reduced from ca. 20 Myr to ca. 4 Myr. The sedimentary gap up to the Illawarra Reversal (ca. 265 Ma after Isozaki 2009; 266.66 ± 0.76 Ma after Hounslow and Balabanov 2018; base of Upper Rotliegend II) therefore has to be extended to > 25 Myr. This result requires a new view on the early evolution of the Thuringian Forest Basin. The sedimentary hiatus, which can extend locally to 30 Myr in Northern Germany (e.g., between Permian volcanics and the Wustrow Member as the oldest Permian sediment), is at least partially caused by volcano-topographic features (morphology) besides intrabasinal tectonics according to Geißler et al. (2008). Further work is required to evaluate this hiatus in sedimentation for the TFB region as well.

Comparison to biostratigraphic data

The modern state of biostratigraphy in the continental basins of Pangea has been summarized by Schneider et al. (2020). The authors describe "biostratigraphic timelines" which are calibrated for Europe and North America by marine zone fossils and are dated for certain levels by radioisotopic zircon ages (including U–Pb CA–ID–TIMS zircon ages) from the Bashkirian (early Pennsylvanian: ca. 319 Ma) to the late Asselian (early Cisuralian: ca. 295 Ma). On this basis, stratigraphic correlations can be done at a local and regional scale. However, there are only a few continental basins at the Pangea margins that are well linked to the global marine standard biostratigraphy. Accordingly, more chronostratigraphic data from Pangea continental basins are urgently needed.

In the TFB, biostratigraphy is well investigated in the sedimentary record. Collecting biostratigraphic data (occurrences) and evaluating biostratigraphic events (first and last appearances) have been used to establish biostratigraphic zoning for insects, especially cockroach wings, for amphibians, vertebrate foot prints and conchostraca as well. However, the correlation with biostratigraphic data in continental Carboniferous and Permian basins is partially problematic (e.g., Schneider et al. 2020). Comparison of Fig. 2 of Schneider et al. (2020) with our new age data for the formations near the Carboniferous–Permian boundary (Möhrenbach Fm. plus Ilmenau Fm. = Gehren subgroup) indicates that both datasets are compatible. However, contradictory interpretations are obtained for the Rotterode Formation: According to our new ages, the Rotterode Formation corresponds to the Asselian Stage while Schneider et al. (2020) place the Rotterode Formation in the Artinskian Stage.

Schneider and Werneburg (2006, 2012) biostratigraphically correlated the Ilmtal fossiliferous horizon in the Möhrenbach Formation (letter B in Fig. 2 and Fig. 6) with the Breitenbach Formation (Saar–Nahe Basin) and the Wettin Subformation (Saale Basin) on the basis of index fossils of the *Branchierpeton saalensis–Apateon intermedius* assemblage zone (amphibians) and of the *Sysciophlebia euglyptica–Syscioblatta dohrni* assemblage zone (insect wings). Schneider et al. (2020) have inferred the late Stephanian (late Gzhelian) time from a zircon SHRIMP age of an intrusive rhyolite near Halle (Breitkreuz et al. 2009). The Stephanian age is also confirmed here by the age for the Kickelhahn Rhyolite (Ilmenau Formation).

The next amphibian biozone following upward, i.e., *Apateon dracyensis–Melanerpeton sembachense* assemblage zone comes from the Sembach fossiliferous horizon near the top of the Ilmenau Formation (letter D in Figs. 2 and 6) and is also reported from the Muse Formation near Dracy St. Loup (Autun basin, France). The upper part of the Muse oil shale is dated between 298.6 ± 0.4 Ma and 298.0 ± 0.4 Ma by the U–Pb CA–ID–TIMS zircon age method (Pellenard et al. 2017; Fig. 6). This fits well to the 299.3 ± 0.3 Ma age of the Kickelhahn Rhyolite when taking into account that the Sembach Horizon is situated at the top of the Ilmenau

Formation and that the Kickelhahn Rhyolite has a somewhat lower position.

Furthermore, the *Sysciophlebia balteata–Spiloblattina homigtalensis* a.z. (insect zone 7), known from the lower Goldlauter Formation in the TFB (letter F in Fig. 2 and Fig. 6), was also discovered in the Ričany Formation, Boskovice Furrow (Czech Republic) (Schneider and Werneburg 2012). There, at the top of the underlying formation, a tuff yielded a CA–ID–TIMS U–Pb zircon age of 298.9 ± 0.4 Ma (Opluštil et al. 2017; Fig. 6). This age stands approximately for the *Sysciophlebia balteata–Spiloblattina homigtalensis* assemblage zone, which had been established in the TFB section by Schneider and Werneburg (2012).

The Goldlauter Formation comprises amphibian zone 5, i.e., *Branchierpeton reinholdi–Apateon flagrifera flagrifera–Melanerpeton eisfeldi* assemblage zone of Werneburg in Schneider et al. (2020) (letters F and G in Figs. 2 and 6). There are no precise radiometric ages for this biostratigraphic zone (Fig. 6).

An important amphibian biozone occurs in the uppermost part of the Oberhof Formation (amphibian zone 7 in Schneider et al. 2020, formerly zone 8 in Schneider and Werneburg 2012, Fig. 8) termed the *Melanerpeton pusillum–Melanerpeton gracile* assemblage zone, found in the Wintersbrunn fossiliferous horizon [syn. Upper *Protriton* Horizon (letter I in Figs. 2 and 6)]. The evidence of this biozone is widespread. It is reported from the Niederhäslich Formation (Döhlen Basin, Saxony), the Schöneck Formation (Hessian Basins), the Humberg Horizon (top of Meisenheim Formation, Saar–Nahe Basin), from several French basins and from the Olevětín Member (Broumov Formation, Intrasudetic Basin) as well (Fig. 6). In the Intrasudetic Basin, this biozone is found in the Ruprechtice limestone horizon in the middle part of the Olevětín Member. Below, at the top of the Nowaruda Member, there occurs the Vraní hory Rhyolite, which is dated by the CA–ID–TIMS U–Pb method at 297.1 ± 0.3 Ma (Opluštil et al. 2016). This is in good agreement with samples 2 and 3 from the Oberhof Formation and sample 1 from the Rotterode Formation of the TFB (Fig. 6). Approximately, 70 m of clastic deposits was accumulated between the Vraní hory Rhyolite and the Ruprechtice Horizon.

The amphibian zone 7 is situated in a median level between the uppermost Older Rhyolite of the Oberhof Formation represented by samples 2 and 3 and the Komberg Rhyolite of the Rotterode Formation (sample 1). Hence, the age of this biozone can be estimated at about 296 Ma from our data.

Conclusions

We report the first investigation by the U–Pb CA–ID–TIMS method of a Stephanian to early Permian (lower Rotliegend) profile in the Thuringian Forest Basin. We draw the following conclusions.

1. First, the results fulfill the expectation that the ages change in the same order as the lithostratigraphic sequence. That is, formations following one another in the order given by lithological mapping yielded zircon ages from older to younger in the same order. Sample 4 is an exception that can be explained by the local tectonics of this sample site.
2. New geochronological results for the Ilmenau Formation (sample 5) and the Oberhof Formation (samples 2 and 3) indicate an age difference of 2.5 Myr between both formations, indicating a ca. 2.5 Myr quiescent magmatic period for the predominantly sedimentary Manebach and Goldlauter Formations. This is in accordance with different biostratigraphic zones. However, still-existing discrepancies between biostratigraphy and geochronology have to be resolved by further geochronological dating and additional paleobiological data.
3. The zircon ages of sample 5 (Kickelhahn Rhyolite, Ilmenau Formation) and the two rhyolite samples (samples 6 and 7, Möhrenbach Formation) are very close to the internationally valid chronostratigraphic Carboniferous-Permian boundary (International Chronostratigraphic Chart 2019) at 298.90 ± 0.15 Ma. Based on the new Kickelhahn Rhyolite zircon age, we assume that the position of the C–P boundary should be located at the base of the Manebach Formation. Consequently, the position of the C–P boundary in the TFB could be established more precisely compared to previous estimates.
4. Compared to earlier concepts, the new zircon ages indicate that the total duration of the volcanic activity in the TFB was considerably shorter. Whereas previously an age interval between 295 and 275 Ma was expected for the whole volcanic period in the TFB, now the range is reduced to a period from ca. 300 Ma (Möhrenbach Formation) to ca. 296 Ma (Rotterode Formation). Consequently, the total duration of volcanic activity is shortened from ca. 20 Myr to ca. 4 Myr. We consider the pre-treatment of the dated zircons by chemical abrasion an important procedure in removing zircon parts with strong Pb loss, e.g., due to late magmatic–hydrothermal activities, that resulted in exceedingly young ages in previous studies.
5. Consequently, the possible time span from the early Permian volcanic rocks (top Rotterode Formation) up to the Illawarra Reversal has to be extended to ca. 30 Myr. This

result requires a new view on the evolution of the TFB. This stratigraphic interval can cover 25–30 Myr in parts of the external Variscides.

6. Our newly obtained ages of the dated TFB formations that contain important biostratigraphic fossils can be used as time marks for certain biostratigraphic zones in other continental late Carboniferous–early Permian basins.
7. In the future, the chronostratigraphic sequence in the Thuringian Forest could be even more precisely defined by dating the Inselsberg and/or Heuberg Rhyolite as a mark for the base of the Oberhof Formation, and the Elgersburg Rhyolite as a mark for the youngest rhyolite. In addition, new age data from the other continental basins are urgently needed, in particular from the Saar–Nahe Basin, the Saale Basin near Halle and the Chemnitz Basin. Such new data will allow the definition of volcanic–subvolcanic–plutonic complexes as cogenetic systems and the assessment of their geochemical signatures, thermal history, and magmatic–hydrothermal evolution in an integrated way.

Acknowledgements We thank Paul Fugmann and Sandra Urban for their help with sample preparation in the laboratory of the Institute of Geosciences, University Jena. U. Linnemann (Senckenberg Naturhistorische Sammlungen Dresden), R. Rößler and S. Trümper (Museum für Naturkunde Chemnitz) agreed that we mention the dating of a tuff layer of the Manebach Formation from a preliminary excavation report in the text and in Fig. 6. This is highly acknowledged. We thank J. Davies, J. Schneider, and V. Lorenz for constructive reviews and substantial improvement of the manuscript.

Author contributions All authors contributed to the study conception and design. Material sampling and preparation was performed by HL and RG. Methodology of zircon dating: MT. Analysis (zircon dating) was performed by AK and MT. The first draft of the manuscript was written by HL and all authors commented on previous versions of the manuscript. All authors read and approved the final manuscript.

Funding Open Access funding enabled and organized by Projekt DEAL.

References

Andreas D (2014) Der Thüringer Wald im Zeitraum der Stefan-Unterperm-Entwicklung—ein Abschnitt der Zentraleuropäischen N-S-Riftzone innerhalb des Mitteleuropäischen Großschollenscharniers. Freiberger Forschungshefte C 547:181

Andreas D, Enderlein F, Judersleben G, Jungwirth J, Mädler J, Michael J, Voigt H (1974) Siles und Rotliegendes im Thüringer Wald und seinem südöstlichen Vorland. In: Hoppe W, Seidel G (eds) Geologie von Thüringen. Gotha, Leipzig, pp 356–449

Andreas D, Haubold H (1975) Die biostratigraphische Untergliederung des Autun (Unteres Perm) im mittleren Thüringer Wald. Schriftenr geol Wiss 3:5–86, Berlin

Andreas D, Lützner H (2009) Schichtenfolge und Paläotektonik des Rotliegenden im mittleren Thüringer Wald zwischen Friedrichroda und Steinbach-Hallenberg. Geowiss Mitt Thüringen 13:141–161, Jena

Bankwitz, P, Bankwitz E (2003) Proterozoikum Schwarzburger Antiklinorium. In: Seidel G (ed) Geologie von Thüringen, Abschnitt 4.2. 52–87; Schweizerbart

Bankwitz P, Kaemmel T (1957) Das Thüringer Hauptgranitmassiv und sein südlicher Rahmen. Abh Geotektonik 12:1–37

Barthel M, Rößler R (2010) Seismite aus dem Rotliegend des Thüringer Waldes Sedimentation und Fossilführung der Tonsteine der Oberen Gehren-Formation δ. Veröffentlichungen Naturhistor Museum Schleusingen 7(8):53–64

Benek R, Kramer W, McCann T, Scheck M, Negendank JFW, Korich D, Huebscher H-D, Bayer U (1996) Permo-Carboniferous magmatism of the Northeast German Basin. Tectonophysics 266:379–404

Beyschlag F (1895) Überblick über die geologische Zusammensetzung des Thüringer Waldes, in Sonderheit des Rotliegenden desselben, unter Vorlegung einer neuen geologischen Übersichtskarte im Maßstab 1: 100.000. Z Dt Geol Ges 47:596–607

Black LP, Kamo SL, Allen CM, Aleinikoff JN, Davies DW, Korsch RJ, Foudoulis C (2003) TEMORA 1: a new zircon standard for Phanerozoic U–Pb geochronology. Chem Geol 200:155–170

Boy JA, Haneke J, Kowalczyk G, Lorenz V, Schindler T, Stollhofen H, Thum H (2012) Rotliegend im Saar-Nahe-Becken, am Taunus-Südrand und im nördlichen Oberrheingraben.—In: Deutsche Stratigraphische Kommission (Hrsg): Stratigraphie von Deutschland X. Rotliegend. Teil I: Innervariscische Becken. Schriftenr Dt Ges Geowiss Heft 61:254–377

Breitkreuz C, Kennedy A (1999) Magmatic flare-up at the Carboniferous/Permian boundary in the NE German basin revealed by SHRIMP zircon ages. Tectonophysics 302:307–326

Breitkreuz C, Mock A (2004) Are laccolith complexes characteristic of transtensional basin systems? Examples from the Permo-Carboniferous of Central Europe. In: Breitkreuz C, Petford N (eds) Physical geology of high-level magmatic systems. J Geol Soc, Lond Spec Publ 234:13–31

Breitkreuz C, Kennedy A, Geißler M, Ehling B-C, Kopp J, Muszynski A, Protas A, Stouge S (2007) Far Eastern Avalonia: Its chronostratigraphic structure revealed by SHRIMP zircon ages from Upper Carboniferous to Lower Permian volcanic rocks (drill cores from Germany, Poland, and Denmark), In: Linnemann U, Nance RD, Kraft P, and Zulauf G, (eds) The evolution of the Rheic Ocean: From Avalonian-Cadomian active margin to Alleghenian-Variscan collision: Geol Soc, Amer, Spec Paper 423:173–190

Breitkreuz C, Ehling B-C, Sergeev S (2009) Chronological evolution of an intrusive/ extrusive system: the Late Paleozoic Halle Volcanic Complex in the northeastern Saale Basin (Germany). Z Dt Ges Geowiss 160(2):173–190

Condon DJ, Schoene B, McLean NM, Bowring SA, Parrish RR (2015) Metrology and traceability of U–Pb isotope dilution

geochronology (EARTHTIME Tracer Calibration Part I). Geochim Cosmochim Acta 164:464–480
Deubel F (1960) Das Untere Perm in Thüringen und angrenzenden Gebieten. Wiss Zeitschr Friedrich Schiller-Univ Jena, Math Naturwiss Reihe 9:409–448
Doblas M, Oyarzun R, López-Ruiz J, Cebría JM, Youbi N, Mahecha V, Lago M, Pocoví A, Cabanis B (1998) Permo-Carboniferous volcanism in Europe and northwest Africa: a superplume exhaust valve in the centre of Pangaea? J Afr Earth Sci 26(1):89–99
Doglioni C, D'Agostino N, Mariotti G et al (1998) Normal faulting vs regional subsidence and sedimentation rate. Mar Petrol Geol 15:737–750
Eberth DA, Berman DS, Sumida SS, Hopf H (2000) Lower Permian terrestrial environments and vertebrate paleoecology of the Tambach Basin (Thüringen, Central Germany), the Uplands Holy Grail. Palaios 15:293–313
Einsele G (1992) Sedimentary basins: evolution, facies, and sediment budget. Springer Verlag, Berlin
Enderlein F, Ziegenhardt W (1975) Geologische Karte der DDR 1: 25000, Blatt 5230 Gräfenroda (Oberhof). Zentral Geol Inst, Berlin
Gast R, Gundlach T (2006) Permian strike slip and extensional tectonics in Lower Saxony Germany. Z Dt Ges Geowiss 157(1):41–56
Gebhardt U, Lützner H, Ehling B-C, Schneider JW, Voigt S, Walther H (2018) Comments on the Stratigraphical Table of Germany 2016—Rotliegend Version B. Z Dt Ges Geowiss 169(2):129–137
Geißler M, Breitkreuz C, Kiersnowski H (2008) Permian Basin (NE Germany, W Poland): facies distribution and volcano-topographic hiati. Int J Earth Sci (Geol Rundsch) 97:973–989. https://doi.org/10.1007/s00531-007-0288-6
Goll M, Lippolt HJ (2001) Biotit-Geochronologie (40Arrad/K, 40Arrad/39ArK, 87Srrad/87Rb) spätvariszischer Magmatite des Thüringer Waldes. N Jb Geol Abh 222:353–405
Gothan W (1928) Über Äquivalente der Wettiner Schichten im Thüringer Walde. Z Dt Geol Ges 79:121–123
Hoffmann U, Breitkreuz C, Breiter K, Sergeev S, Stanek K, Tichomirowa M (2013) Carboniferous–Permian volcanic evolution in Central Europe—U/Pb ages of volcanic rocks in Saxony (Germany) and northern Bohemia (Czech Republic). Int J Earth Sci (Geol Rundsch) 102:73–99. https://doi.org/10.1007/s00531-012-0791-2
Hoth K, Huebscher H-D, Korich D, Gabriel W, Enderlein F (1993) Die Lithostratigraphie der permokarbonischen Effusiva im Zentralabschnitt der Mitteleuropäischen Senke—Der permokarbone Vulkanismus im Zentralabschnitt der Mitteleuropäischen Senke. Geol Jb A 131:179–196
Hounslow MW, Balabanov YP (2018) A geomagnetic polarity timescale for the Permian, calibrated to stage boundaries. Geological Society, London (**Permian GPTS**)
International Chronostratigraphic Chart 2019. www.stratigraphy.org. International Commission on Stratigraphy. 2019-05
Isozaki Y (2009) Illawarra reversal: the fingerprint of a superplume that triggered Pangean breakup and the end-Guadalupian (Permian) mass extinction. Gondwana Res 15:421–432. https://doi.org/10.1016/j.gr.2008.12.007
Jaffey AH, Flynn KF, Glendenin LE, Bentley WC, Essling AM (1971) Precision measurement of half-lives and specific activities of ^{235}U and ^{238}U. Phys Rev C. https://doi.org/10.1103/PhysRevC.4.1889
Kroner U, Roscher M, Romer RL (2016) Ancient plate kinematics derived from the deformation of continental crust: Paleo- and Neo-Tethys opening coeval with prolonged Gondwana–Laurussia convergence. Tectonophysics 681:220–233. https://doi.org/10.1016/j.tecto.2016.03.034
Kroner U, Stephan T, Romer RL, Roscher M (2020) Paleozoic plate kinematics during the Pannotia–Pangea supercontinent cycle. Geol Soc Lond Spec Publ. https://doi.org/10.1144/SP503-2020-15
Lippolt H-J, Mädler J, Goll M (2009) Interpretation von 40Ar/39Ar-Altersbestimmungen an Gesteins- und Plagioklas-Präparaten aus dem Höhenberg-Lagergang im Thüringer Wald. Geowiss Mitt Thüringen 13:99–140
Lorenz V, Haneke J (2004) Relationship between diatreme, dykes, sills, laccoliths, intrusive-extrusive domes, lava flows and tephra deposits with unconsolidated water-saturated sediments in the late Variscan intermontane Saar-Nahe Basin, SW Germany. In: Breitkreutz C, Petford N (eds) Physical Geology of High-Level Magmatic Systems. Geol Soc, London, Spec Publ 234:75–124
Lorenz V, Nicholls IA (1976) The Permocarboniferous basin and range province of Europe. An application of plate tectonics. In: Falke H (ed) The continental Permian in Central, West and South Europe 1. Reidel, , Dordrecht, pp 312–342
Lorenz V, Nicholls IA (1984) Plate and intraplate processes of Hercynian Europe during the Late Paleozoic. Tectonophysics 107:25–56
Loretz H, Scheibe R, Zimmermann E (1908) Erläuterungen zur Geologischen Karte von Preußen und den Thüringischen Staaten, Lfg. 64, Blatt Ilmenau. P 183
Lützner H, Kowalczyk G (2012) Stratigraphie von Deutschland X. Rotliegend. Teil I: innervariscische becken. Schriftenr Dt Ges Geowiss 61:883
Lützner H, Littmann S, Mädler S, Romer RL, Schneider JW (2007) Radiometric and biostratigraphic data of the continental Permocarboniferous reference-section Thüringer Wald, Germany. In: Wong Th E (ed) Proc. of the 15th Int. Congr. on Carboniferous and Permian Stratigraphy, Utrecht, the Netherlands, 10–16 August 2003:161–174
Lützner H, Andreas D, Schneider JW, Voigt S, Werneburg R (2012) Stefan und Rotliegend im Thüringer Wald und seiner Umgebung. In: Deutsche Stratigraphische Kommission (Hrsg, Koordination und Redaktion: Lützner H, Kowalczyk G für die Subkommission Perm-Trias): Stratigraphie von Deutschland X. Rotliegend. Teil I: Innervariscische Becken. Schriftenr Dt Ges Geowiss 61:418–487
Martens T (2001) Paläontologie, Biostratigraphie und Paläogeographie der Tambach-Formation (Oberrotliegend, Unterperm) im Thüringer Wald—ein Überblick. Beiträge Geol Thüring NF 8:131–212
Martens, T (2012) Biostratigraphie der Conchostraca (Branchiopoda, Crustacea) des Rotliegend. In: Deutsche Stratigraphische Kommission (Hrsg, Koordination und Redaktion: Lützner H, Kowalczyk G für die Subkommission Perm-Trias): Stratigraphie von Deutschland X. Rotliegend. Teil I: Innervariscische Becken. Schriftenr Dt Ges Geowiss, 2012, Heft 61:98–109
Mattinson JM (2005) Zircon U–Pb chemical abrasion ("CA-TIMS") method: combined annealing and multi-step partial dissolution analysis for improved precision and accuracy of zircon ages. Chem Geol 220:47–66
Marx J (1995) Permokarbonischer vulkanismus in niedersachsen. Zentralbl Geol Paläont Teil I 1993(9/10):1429–1442
Marx J, Huebscher H-D, Hoth K, Korich D, Kramer W (1995) Vulkanostratigraphie und Geochemie der Eruptivkomplexe. Stratigraphie von Deutschland I—Norddeutsches Rotliegendbecken. Cour Forsch Senckenb 183:54–83
Mazur S, Aleksandrowski P, Turniak K, Krzemiński L, Mastalerz K, Górecka-Nowak A, Kurowski L, Krzywiec P, Żelaźniewicz A, Fanning MC (2010) Uplift and late orogenic deformation of the Central European Variscan belt as revealed by sediment provenance and structural record in the Carboniferous foreland of western Poland. Int J Earth Sci 99:47–64
McCann T, Pascal C, Timmerman MJ, Krzywiec P, López-Gómez J, Wetzel L, Krawczyk CM, Rieke H, Lamarche J (2006) Post-Variscan (end Carboniferous-Early Permian) basin evolution in Western and Central Europe. Geol Soc Lond Mem 32:355–388
McLean NM, Condon DJ, Schoene B, Bowring SA (2015) Evaluating uncertainties in the calibration of isotopic reference materials and

multi-element isotopic tracers (EARTHTIME Tracer Calibration Part II). Geochim Cosmochim Acta 164:481–501
Meinel G (2003): Magmatismus und Metamorphose. In: Seidel G (ed) Geologie von Thüringen, 207–214; Schweizerbart
Menning M, Katzung G, Lützner H (1988) Magnetostratigraphic investigation of the Rotliegendes (300–252 Ma) of Central Europe. Z Geol Wiss 16:1045–1063
Menning, M, Bachtadse V (2012): Magnetostratigraphie und globale Korrelation des Rotliegend innervarscischer Becken. In: Deutsche Stratigraphische Kommission (Hrsg, Koordination und Redaktion: Lützner H, Kowalczyk G für die Subkommission Perm-Trias): Stratigraphie von Deutschland X. Rotliegend. Teil I: Innervariscische Becken. Schriftenr Dt Ges Geowiss, Heft 61:176–203
Menning M, Hendrich A, Deutsche Stratigraphische Kommission (2016) Stratigraphische Tabelle von Deutschland 2016 (STD 2016)
Michael J (1972) Zur Paläogeographie der Gehrener Schichten im südöstlichen Thüringer Wald. Ber Dt Ges Geol Wiss A 17:835–847
Miller J, Matzel J, Miller C, Burgess S, Miller R (2007) Zircon growth and recycling during the assembly of large, composite arc plutons. J Volcanol Geotherm Res 167:282–299
Neumann E-R, Wilson M, Heeremans M, Spencer EA, Obst K, Timmerman MJ, Kirstein L (2004) Carboniferous–Permian rifting and magmatism in southern Scandinavia, the North Sea and northern Germany: a review. Geol Soc Lond Spec Publ 223:11–40
Obst K, Katzung G (2000) Die magmatischen Gänge am Südrand des Kristallins von Ruhla-Brotterode (Thüringer Wald)—Herkunft der Magmen, Aufstieg und Platznahme im variszischen Spannungsfeld. Z Dt Geol Ges 151:441–470
Obst K, Katzung G, Hammer J (1999) Dating of the Late Autunian basic magmatism in the Thuringian Forest. N Jb Geol Paläont Mh Jg 1999:1–10
Opluštil S, Schmitz M, Kachlík V, Štamberg S (2016) Re-assessment of lithostratigraphy, biostratigraphy, and volcanic activity of the Late Paleozoic Intra-Sudetic, Krkonoše-Piedmont and Mnichovo Hradište basins (Czech Republic) based on new U–Pb CA-ID-TIMS ages. Bull Geosci 91(2):399–432
Opluštil S, Jirásek J, Schmitz M, Matýsek D (2017) Biotic changes around the radioisotopically constrained Carboniferous–Permian boundary in the Boskovice Basin (Czech Republic). Bull Geosci 92(1):95–122
Patzelt G (1966) Bau und Schichtenfolge der Asbach-Rotteröder Mulde (Thüringerwald) nach neueren Kartierungsergebnissen. Hallesches Jb Mitteldeutsch Erdgesch 7:39–60
Paul J (2012) Das Klima des Rotliegend. In: Deutsche Stratigraphische Kommission (Hrsg, Koordination und Redaktion: Lützner H, Kowalczyk G für die Subkommission Perm-Trias): Stratigraphie von Deutschland X. Rotliegend. Teil I: Innervariscische Becken. Schriftenreihe der Deutschen Gesellschaft für Geowissenschaften, Heft 61:731–742
Pellenard P, Gand G, Schmitz M, Galtier J, Broutin J, Stéyer J-S (2017) High-precision U-Pb zircon ages for explosive volcanism calibrating the NW European continental Autunian stratotype. Gondwana Res 51:118–136
Plein E (1993) Bemerkungen zum Ablauf der paläogeographischen Entwicklung im Stefan und Rotliegend des Norddeutschen Beckens. Geol Jb A 131:99–116
Ramezani J, Schmitz MD, Davydov VI, Bowring SA, Snyder WS, Northrup CJ (2007) High-precision U–Pb zircon age constraints on the Carboniferous–Permian boundary in the southern Urals stratotype. Earth Planet Sci Lett 256:244–257
Roscher M, Schneider JW (2006) Early Pennsylvania to Late Permian climatic development of Central Europe in a regional and global context. In: Lucas SG, Schneider JW, Cassinis G (eds) Non-marine Permian Chronology and Correllation. Geol Soc Lond Spec Publ 265:95–136
Schaltegger U, Schmitt AK, Horstwood MSA (2015) U–Th–Pb zircon geochronology by ID-TIMS, SIMS, and laser ablation ICP-MS: recipes, interpretations, and opportunities. Chem Geol 402:89–110
Schmiedel T, Breitkreuz C, Görz I, Ehling B-C (2015) Geometry of laccolith margins: 2D and 3D models of the Late Paleozoic Halle Volcanic Complex (Germany). Int J Earth Sci 104:323–333
Schneider JW (1996) Biostratigraphie des kontinentalen Oberkarbon und Perm im Thüringer Wald, SW Saale-Senke—Stand und Probleme. Beiträge zur Geologie von Thüringen Neue Folge 3:121–151
Schneider JW, Werneburg R (2006) Insect biostratigraphy of the European continental Late Pennsylvanian and Early Permian. In: Lucas SG, Cassinis G, Schneider JW (eds) Non-marine Permian biostratigraphy and biochronology. Geol Soc Lond, Spec Publ 265:325–336
Schneider JW, Werneburg R (2012) Biostratigraphie des Rotliegend mit Insekten und Amphibien. In: Deutsche Stratigraphische Kommission (Hrsg.; Koordination und Redaktion: H. Lützner und G. Kowalczyk für die Subkommission Perm-Trias): Stratigraphie von Deutschland X. Rotliegend. Teil I: Innervariscische Becken. Schriftenr Dt Ges Geowiss Heft 61:110–142
Schneider JW, Spencer GL, Scholze F, Voigt S, Marchetti L, Klein H, Opluštil S, Werneburg R, Golubev VK, Barrick JE, Nemyrovska T, Ronchi A, Day MO, Silantiev VV, Rößler R, Saber H, Linnemann U, Zharinova V, Shen Sh (2020) Late Paleozoic—early Mesozoic continental biostratigraphy—links to the Standard Global Chronostratigraphic Scale. Palaeoworld 29:186–238. https://doi.org/10.1016/j.palwor.2019.09.001
Schoene B, Crowley JL, Condon DJ, Schmitz MD, Bowring SA (2006) Reassessing the uranium decay constants for geochronology using ID-TIMS U–Pb data. Geochim Cosmochim Acta 70:426–445
Stacey JS, Kramers JD (1975) Approximation of terrestrial lead isotope evolution by a two-stage model. Earth Planet Sci Lett 26:207–221
Thomson SN, Zeh A (2000) Fission track thermochronology of the Ruhla Crystalline Complex: new constraints on the post-Variscan thermal evolution of the NW Saxo-Bohemian Massif. Tectonophysics 324:17–35
Tichomirowa M, Käßner A, Sperner B, Lapp M, Leonhardt D, Linnemann U, Münker C, Ovtcharova M, Pfänder JA, Schaltegger U, Sergeev S, von Quadt A, Whitehouse M (2019) Dating multiply overprinted granites: the effect of protracted magmatism and fluid flow on dating systems (zircon U-Pb: SHRIMP/SIMS, LA-ICP-MS, CA-ID-TIMS; and Rb–Sr, Ar–Ar)—Granites from the Western Erzgebirge (Bohemian Massif, Germany). Chem Geol 519:11–38. https://doi.org/10.1016/j.chemgeo.2019.04.024
Timmerman MJ (2004) Timing, geodynamic setting and character of Permo-Carboniferous magmatism in the foreland of the Variscan Orogen, NW Europe. In: Wilson M, Neumann E-R, Davies GR, Timmerman MJ, Heeremans M, Larsen BT (eds) Permo-Carboniferous Magmatism and Rifting in Europe. Geol Soc Lond Spec Publ 223:41–74
Timmerman MJ (2008) Paleozoic magmatism. In: McCann T (ed) The geology of Central Europe, Volume 1. Precambrian and Paleozoic. Geol Soc Lond, pp 665–748
Trümper S, Hellwig A, Rößler R (2020) Neue Forschungen an der Wiege der Paläobotanik. GMIT Geowiss Mitt 79:22–23
Van Wees J-D, Stephenson RA, Ziegler PA, Bayer U, McCann T, Dadlez R, Gaupp R, Narkiewicz M, Bitzer F, Scheck M (2000) On the origin of the Southern Permian Basin, Central Europe. Mar Petrol Geol 17:43–59
von Seckendorff V, Arz C, Lorenz V (2004) Magmatism of the late Variscan intermontane Saar-Nahe Basin (Germany): a review. In: Wilson M, Neumann EG, Davies GR, Timmerman MJ,

Heeremans M, Larsen BT (eds) Permo–Carboniferous magmatism and rifting in Europe. Geol Soc, Lond, Spec Publ 223:361–391

von Seckendorff V (2012) Der Magmatismus in und zwischen den spätvariscischen permokarbonen Sedimentbecken in Deutschland. In: Deutsche Stratigraphische Kommission (Hrsg; Koordination und Redaktion: Lützner H, Kowalczyk G für die Subkommission Perm-Trias): Stratigraphie von Deutschland X. Rotliegend. Teil I: Innervariscische Becken.Schriftenr Dt Ges Geowiss, Heft 61:760–877

Wiedenbeck M, Alle P, Corfu F, Griffin WL, Meier M, Oberli F, von Quadt A, Roddick JC, Spiegel W (1995) Three natural zircon standards for U–Th–Pb, Lu–Hf, trace element and REE analysis. Geostand Newslett 19:1–23

Willcock MAW, Cas RAF, Giordano G, Morelli C (2013) The eruption, pyroclastic flow behaviour, and caldera infilling processes of the extremely large volume (> 1290 km^3), intra- to extra-caldera, Permian Ora (Ignimbrite) Formation, Southern Alps, Italy. J Volc Geotherm Res 265:102–126

Yeats RS (1978) Neogene acceleration of subsidence rates in southern California. Geology 6(8):456–460

Zeh A, Brätz H (2000) Radiometrische und morphologische Untersuchungen an Zirkonen aus Granitporphyren, Rhyolithen und Granitgeröllen des nordwestlichen Thüringer Waldes. Z Dt Geol Ges 151:187–206

Zeh A, Cosca MA, Brätz H, Okrusch M, Tichomirowa M (2000) Simultaneous horst-basin formation and magmatism during Late Variscan transtension: evidence from 40Ar/39Ar and 207Pb/206Pb geochronology in the Ruhla Crystalline Complex. Int J Earth Sci 89:52–71

Ziegler PA (1990) Geological atlas of western and Central Europe 1990. Blackwell, Oxford, p 239